Operation and theory of a driven single-mode electron cyclotron maser

A. H. McCurdy*
Omega-P, Inc., 2008 Yale Station, New Haven, Connecticut 06520

A. K. Ganguly and C. M. Armstrong
Electronics Science and Technology Division, Naval Research Laboratory, Washington, D.C. 20375
(Received 24 October 1988; revised manuscript received 27 January 1989)

A study is made of the operation of the electron cyclotron resonance maser (ECRM), when subjected to an external rf signal. The signal is introduced both via direct injection through a coupling hole in the oscillator and by modulating the electron beam in separate cavities, upstream of the oscillator. Experiments using both one and two "prebunching" cavities are reported. It is experimentally found that the gyromonotron, a specific embodiment of the ECRM, can be phase locked by premodulating the electron beam at drive power levels more than two orders of magnitude below that predicted by Adler's widely applicable theory for single-cavity oscillators. A perturbation theory is used to predict the phase-locking frequency band for a gyromonotron with any number of prebunching cavities. The predictions of this theory agree with the experimental results for two- and three-cavity phase locking. An investigation is made into the general amplitude and frequency response of the ECRM to an applied external signal. Experimentally, three distinct regions of qualitatively different ECRM behavior are noted: soft excitation, which is free, self-excited oscillation; hard excitation, where the oscillation requires an external impulse for startup; and amplifier, in which the output power level and frequency are linearly related to the drive in the small-signal regime.

I. INTRODUCTION

The electron cyclotron resonance maser (ECRM) is a microwave device capable of oscillation or amplification in different regimes of its parameter space. The ECRM interaction consists of a coupling of the fast right-hand circularly polarized cyclotron electron beam wave with a superluminous electromagnetic wave. In its oscillator variant, the ECRM has proven to be an efficient, powerful source of coherent radiation at centimeter to millimeter wavelengths. One practical embodiment of the ECRM utilizing a magnetron injection gun (MIG) (generating an annular gyrating electron beam) with a cavity oscillator (with cross section near the waveguide cutoff) is called the gyromonotron.[1] Since no intricate slow-wave structure is required to couple the electromagnetic wave to the beam wave the gyromonotron avoids electrical breakdown problems and alleviates thermal-wall loading at high frequencies and powers. Gyromonotrons have produced microsecond pulse powers over 600 kW at frequencies well over 100 GHz,[2,3] and cw powers of 200 kW at 140 GHz.[4]

For applications where the requirement on phase coherence is strict, such as is the case with high-energy linear accelerators, an amplifier such as the gyroklystron[5] would be appropriate. Gyroamplifiers,[6] however, have not yet demonstrated the high efficiencies and power output of the oscillators; hence a method of obtaining phase control over the oscillator is of interest.

This paper builds on a previous work[7] in which phase control was achieved by two methods, phase locking and priming. Both of these methods involve injection of a stable external rf signal into the gyromonotron. The signal is coupled into the gyromonotron in one of two ways; direct injection into the oscillator or coupling to the electron beam in a prebunching cavity.[8,9] The prebunching method differs from that of the complex cavity technique[10,11] in that the design of the prebunching cavity prevents self-excited oscillation and an external signal is used. The experimental apparatus and diagnostics are described in Sec. II. A perturbation theory[12] gives the phase-locking frequency bandwidth in the limit of small-frequency difference between the drive signal and free oscillation ($|\omega_0-\omega_d|/\omega_0 \ll 1$) and small drive-to-oscillator power ratio ($P_d/P_0 \ll 1$). This theory is combined with a single-particle, linear analysis of the beam–electromagnetic field interaction in the prebunching cavities[13] to yield a multicavity phase-locking theory. The theory is valid for any number of prebunching cavities and any transverse electric mode. This development is given in Sec. III. The experimental phase-locking results are compared with the small-signal theory in Secs. IV A and IV B.

A variety of oscillator issues are addressed in this paper. The unifying thread is that it is the effects of the external signal which are emphasized when studying each phenomenon. A complete examination of each topic would require far more space than is available. Therefore the following phenomena are described in a more qualitative way and references are given to the more detailed studies.

A brief overview of phase control of the gyromonotron by injection of an external signal during the buildup of oscillation is given in Sec. IV C. A more complete ex-

planation of the phenomenon as well as experimental priming results using the previously described direct injection and prebunching methods are given in Ref. 14.

There have been predictions that the highest efficiency regime of operation for the gyromonotron is below the start oscillation current in the "hard-excitation" regime.[15] The characteristic of this regime is that the gyromonotron requires an initial cavity field amplitude, well above the noise level, in order to oscillate. One of the proposed means of accessing this regime is by adjusting the magnetic field once the oscillation has started. Our experiments show that it is possible to operate in the hard-excitation regime by applying an external signal. These observations and other qualitatively different regimes of ECRM response to external excitation are detailed in Sec. IV D.

Finally, free running, pulsed oscillators tend to be noisy. There is a fair amount of randomness in the start-up time in the pulsed oscillator since the fields build up from rf noise generated by beam-current density fluctuations. Also there is pulse-to-pulse jitter in the oscillation frequency and amplitude due to slight variations in the beam conditions. These noise problems can be somewhat alleviated by injection of a stable external signal. An investigation of noise suppression in the gyromonotron is given elsewhere.[7,14]

II. EXPERIMENTAL APPARATUS

A. Multicavity setup

The experiments are carried out using the Naval Research Lab (NRL) 4.5 GHz, three-cavity gyroklystron[16] configuration which is shown in Fig. 1. A MIG produces a thin annular electron beam which then interacts with the cavity electromagnetic fields. The drift sections between the cavities are cutoff to the 4.5 GHz radiation and provide ~ 30 dB of intercavity isolation. All three cavities are rectangular and operate in the TE_{101} mode. Each cavity is tunable via a movable diaphragm in one of the side walls. In normal gyroklystron amplifier operation the beam conditions are such that all three cavities are below the start oscillation threshold. It is possible to excite an ECRM oscillation in any of the cavities, however, by appropriately profiling the magnetic field along the axis of the device and increasing the perpendicular to parallel velocity ratio α of the beam. Waveguide couples out radiation from each of the cavities in Fig. 1 so that the fields in each cavity can be monitored. The first two cavities are identical in construction (0.9λ in length, $Q_L \approx 650$, $Q_e \approx 1100$, undercoupled), while the third cavity is somewhat longer (1.1λ and $Q_L \approx 300$, $Q_e \approx 375$, overcoupled). Here λ is the free-space wavelength and Q_L and Q_e are the loaded (cold cavity), and external quality factors, respectively.

Since the cavity fields interact with the beam at the fundamental relativistic electron cyclotron frequency an axial magnetostatic field of 1.6 kG is required. The experiment utilizes an electron beam with a 60 Hz repetition rate of 4.0 μsec pulses. The beam voltage is near 30 kV and the beam currents are 5 to 6 A. The beam α is in the range 1.0–1.2 for two- and three-cavity operation but is somewhat higher when an oscillation is excited in cavity no. 1 (~ 1.3–1.5). These values for α are determined from measurements of radiation frequency and beam energy together with the uncoupled dispersion diagrams of the cavity-beam system as well as from theoretically predicted gyroklystron gain in the multicavity situation.

B. Diagnostics

The phase-locking experiments consist of injecting an external rf signal, produced by a stable sweep oscillator and amplifier, into the gyroklystron configuration. Low-pass filters are used on the input and output to prevent harmonic gyromonotron emission from reaching the external apparatus. Isolators on the input of the gyroklystron configuration prevent the fundamental harmonic gyromonotron output from disrupting the drive source. These reduce feedback gyromonotron oscillator power by about a factor of 10^8.

Several diagnostics are used to determine the onset of the phase-locked state. First, the input and output frequencies are monitored by digital frequency meters (a pulse counter measures the output frequency). As the gyromonotron becomes locked, the output frequency shifts to the value of the drive frequency. The fact that the drive frequency remains unchanged throughout the

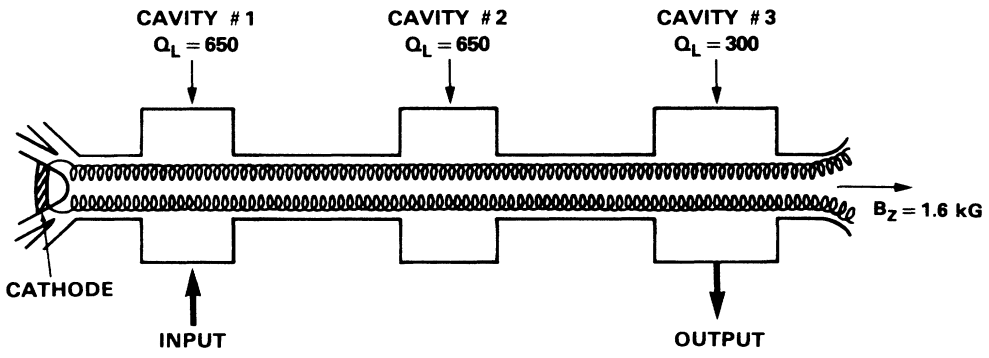

FIG. 1. Three-cavity gyroklystron configuration.

locking process is evidence that the driver is not being locked by the gyromonotron. Second, a spectrum analyzer is used to monitor the frequency content of the gyromonotron output. When the drive signal is sufficiently close in frequency to the oscillation, a peak corresponding to this frequency appears in the output spectrum. As the drive power is increased, the gyromonotron peak merges with the peak at the drive frequency. Third, the drive and output signals are mixed, and the intermediate frequency (IF) output displayed on an oscilloscope. The beat signal, which is present in the unlocked state, discontinuously vanishes as the transition to the locked state takes place. This same phenomenon can be observed directly on a crystal diode as amplitude modulation in the gyromonotron output due to the presence of the two frequencies. Finally a phase discriminator[17] provides a polar display of the change with time of the relative phase between the driver and oscillator. Shifting the phase of the driver and making sure that the oscillator phase follows verifies that the gyromonotron is locked to a constant phase angle with respect to the drive.

III. THEORY

A. Direct-injection phase locking

Phase locking by direct injection of an external signal has been a common method of achieving phase control over oscillators. The first experiments were done on electron tube circuits[18–20] and later on microwave oscillators[21,22] and lasers.[23,24] The phase-locking phenomenon may be observed when an external signal of power P_d and frequency ω_d is applied to an oscillator of power P_0 and frequency ω_0 if the Adler relation[20] is satisfied. This relation has been written in a convenient form for microwave oscillators operating into a matched load by Slater[25]

$$Q_e \frac{|\omega_d-\omega_0|}{\omega_0}\left[\frac{P_0}{P_d}\right]^{1/2}<1\ , \tag{1}$$

where Q_e is the external quality factor of the oscillator cavity. The meaning of Eq. (1) is that at a given frequency separation between the drive signal and the oscillator, the drive-to-oscillator power ratio must exceed a threshold level for phase locking to take place. When the oscillator is phase locked, the oscillation proceeds at the drive frequency and has a constant phase shift from the drive signal.

B. Phase locking by premodulation of the electron beam

An alternative means of coupling the drive signal into the oscillator is via modulation in the gain medium. In a microwave oscillator this means current density modulation in the electron beam. This modulation can be achieved by passing the beam through a separate cavity to which the drive signal is applied. Previous theoretical analysis of this method in a gyromonotron[9,12] has predicted that a smaller drive power would be required to phase lock the free oscillation at a given frequency difference $|\omega_d-\omega_0|$ for electron beam premodulation than for the direct-injection case.

The frequency-locking band of a gyromonotron oscillator driven by an external signal introduced into a single prebunching cavity has been calculated by Manheimer.[12] Here we extend that result to include any number of prebunching cavities and derive an equation for the phase-locking band in the presence of competing modes. This calculation makes the assumptions of weak nonlinearity and small growth rate due to the interaction between the electron beam and the field in the oscillator cavity. The structure of the oscillator cavity mode is assumed to be unperturbed by the presence of the electron beam. Expanding the electromagnetic fields in Slater cavity modes[25] allows equations to be written for the time response of each mode to the drive current. The method of slowly varying amplitude and phase is used to separate the fast-oscillation time scale (rf frequency) from that of the phase-locking process. The steady-state solution to the equation for slowly varying phase gives the locking bandwidth of a given mode in a simple form when the assumption is made that the oscillator power and frequency are close to their free-running values.

1. Determination of the phase-locking bandwidth

The following expansion is used for the TE mode rf cavity fields:

$$\mathbf{E}=\sum_n a_n(t)\mathbf{e}_n,\quad \mathbf{H}=\sum_n b_n(t)\mathbf{h}_n\ ,$$

where n represents a particular combination of m, l, and q, the three eigenvalues in the three-dimensional cavity and $\mathbf{E}$ and $\mathbf{H}$ are real quantities (m and q can be negative). Here the eigenfunctions are

$$\mathbf{e}_n=\nabla\times[f_q(z)\psi_{ml}(\mathbf{r}_\perp)\hat{\mathbf{z}}],\quad \mathbf{h}_n=\frac{1}{k_n}\nabla\times\mathbf{e}_n\ ,$$

where ψ_{ml} satisfies the two-dimensional Helmholtz equation:

$$(\nabla_\perp^2+k_{ml})\psi_{ml}(\mathbf{r}_\perp)=0$$

and the normal derivative of ψ_{ml} vanishes at the conducting portions of the cavity walls. The eigenfunctions are normalized so the coefficients $a_n(t)$ and $b_n(t)$ may be expressed

$$a_n(t)=\int_V d^3r\ \mathbf{E}\cdot\mathbf{e}_n^*,\quad b_n(t)=\int_V d^3r\ \mathbf{H}\cdot\mathbf{h}_n^*\ ,$$

where the integrals are taken over the cavity volume V. The vacuum wave equation describing the evolution in time of the nth mode can be shown to be[25]

$$\left[\frac{1}{c^2}\frac{d^2}{dt^2}+k_n^2\right]a_n(t) = -\mu_0\frac{d}{dt}\left[\int_V d^3r\ \mathbf{J}\cdot\mathbf{e}_n^*-\int_{S'}d^2r(\hat{\mathbf{n}}\times\mathbf{H})\cdot\mathbf{e}_n^*\right] -k_n\int_S d^2r(\hat{\mathbf{n}}\times\mathbf{E})\cdot\mathbf{h}_n^*\ ,$$

where $\hat{\mathbf{n}}$ is the outward normal to the cavity surface. $\mathbf{J}$ (a real quantity) consists of the electronic current inside of the cavity volume. The surfaces S' and S represent insu-

lating and conducting portions of the cavity walls, respectively.

We use the method of slowly varying amplitude and phase to study the transition from a free-running, multimode steady state to a phase-locked oscillation. The time dependence of the electric field is

$$a_n(t)=\tfrac{1}{2}A_n(t)e^{i[\Psi_n(t)+\omega_n t]}+\text{c.c.}$$
$$=\tilde{a}_n(t)+\text{c.c.}\ , \tag{2}$$

where A_n and Ψ_n are slowly varying in time and ω_n is the free-running frequency of the nth mode (including the mode interactions). The instantaneous frequency of the oscillation is $\omega_n+\dot{\Psi}_n$.

The ac beam current is written as a sum of the modulation due to the gyromonotron cavity fields $\mathbf{J}_0$ and that due to the premodulation $\mathbf{J}=\mathbf{J}_{\text{osc}}+\mathbf{J}_{\text{PM}}$. It is assumed that the premodulated current is a first-order quantity (hence small-signal theory can be used in the prebunching section). The expansions for the current are

$$\mathbf{J}_{\text{osc}}(\mathbf{r},t)=\tfrac{1}{2}\sum_n[J_n(t)e^{i[\Psi_n(t)+\omega_n t]}+\text{c.c.}]$$
$$\times\mathbf{e}_n(\mathbf{r})=\tilde{\mathbf{J}}_{\text{osc}}+\text{c.c.}\ ,$$
$$\mathbf{J}_{\text{PM}}(\mathbf{r},t)=\tfrac{1}{2}\mathbf{J}_P(\mathbf{r})e^{i\omega_d t}+\text{c.c.}=\tilde{\mathbf{J}}_P+\text{c.c.}\ , \tag{3}$$

where ω_d is the driving frequency and J_n varies on the same time scale as A_n.

The surface integrals of the wave equation can be written in terms of the cavity quality factors. Assuming that a good conductor comprises surface S and a single waveguide mode propagates into a matched load through the cavity output, the integrals over S and S' may be written (dropping the complex conjugates),

$$\sum_{n'}\frac{(1+i)\omega_n}{c^2k_{n'}Q_0^{nn'}}\frac{d}{dt}\tilde{a}_{n'}(t)$$

and

$$-\epsilon_0\omega_n\sum_{n'}\frac{\tilde{a}_{n'}(t)}{Q_e^{nn'}}\ ,$$

respectively. Here Q_0 is the quality factor due to Ohmic wall losses and Q_e is again the external quality factor. Terms proportional to the small quantities

$$\frac{J}{Q_0},\quad \frac{1}{Q_0Q_e},\quad \frac{d\ln(A)}{dt}\frac{1}{\omega Q},\ \text{and}\ \frac{d\Psi}{dt}\frac{1}{\omega Q}$$

have been neglected. Using these relations in the wave equation (and dropping complex conjugates) the following multimode equation is obtained:

$$\left[\frac{d^2}{dt^2}+c^2k_n^2\right]\tilde{a}_n(t)$$
$$+\omega_n\sum_{n'}\left[\frac{(1+i)k_n}{k_{n'}Q_0^{nn'}}+\frac{1}{Q_e^{nn'}}\right]\frac{d}{dt}\tilde{a}_{n'}(t)$$
$$=-\mu_0c^2\frac{d}{dt}\int_V d^3r(\tilde{\mathbf{J}}_{\text{osc}}+\tilde{\mathbf{J}}_P)\cdot\mathbf{e}_n^*\ . \tag{4}$$

The mode coupling takes place through the cavity losses and the beam current. Substituting Eqs. (2) and (3) into (4) yields an equation whose real and imaginary parts give the frequency and amplitude evolution. The frequency determining equation is

$$\frac{d}{dt}\Psi_n+\frac{1}{2}\left[\omega_n-\frac{1}{A_n}\text{Re}(L)-\frac{\omega_n^{0^2}}{\omega_n}\right]+\frac{\omega_n}{2}\text{Re}(\chi_{\text{osc}_n})$$
$$=-\frac{\omega_n}{2}\text{Re}(\chi_{P_n})\ , \tag{5}$$

where χ_{osc_n} and χ_{P_n} are the electronic susceptibilities of the gyromonotron oscillation and prebunching interactions respectively,

$$\chi_{\text{osc}_n}=-\frac{i}{\omega_n^2\epsilon_0A_n}\int_V d^3r\sum_{n'}\mathbf{e}_{n'}\cdot\mathbf{e}_n^*e^{i[(\omega_{n'}-\omega_n)t+\Psi_{n'}-\Psi_n]}\omega_{n'}J_{n'}(t)=-i\frac{J_n(t)}{\omega_n\epsilon_0A_n}\ ,$$
$$\chi_{P_n}=-\frac{i}{\omega_n^2\epsilon_0A_n}\int_V d^3r\,\mathbf{J}_P\cdot\mathbf{e}_n^*e^{i[(\omega_d-\omega_n)t-\Psi_n]}\omega_d \tag{6}$$

and

$$L=\sum_{n'}\left[\frac{(1+i)k_n}{k_{n'}Q_0^{nn'}}+\frac{1}{Q_e^{nn'}}\right]iA_{n'}\omega_{n'}$$
$$\times e^{i[(\omega_{n'}-\omega_n)t+\Psi_{n'}-\Psi_n]}\ .$$

We have dropped the terms J_n and $\dot{\Psi}_nJ_n$ in arriving at Eq. (5). The cold cavity resonant frequency is designated ω_n^0. Equation (5) is a sequence of equations which determine the effect of the drive signal on each of the electromagnetic modes. χ_{osc_n} may be expanded, in the approximations of quasilinear mode-coupling theory,[26,27] to second order in the field amplitudes:

$$\chi_{\text{osc}_n}\cong\frac{1}{\omega_nA_n}\left[\sum_\sigma A_\sigma e^{i[(\omega_\sigma-\omega_n)t+\Psi_\sigma-\Psi_n]}\alpha_{n\sigma}\right.$$
$$+\sum_\sigma\sum_\nu\sum_\rho A_\sigma A_\nu A_\rho e^{i\Phi_{\sigma\nu\rho n}}\theta_{\sigma\nu\rho n}$$
$$\left.+\cdots\right]\ , \tag{7}$$

where

$$\Phi_{\sigma\nu\rho n}=(\omega_\sigma-\omega_\nu+\omega_\rho-\omega_n)t+\Psi_\sigma-\Psi_\nu+\Psi_\rho-\Psi_n\ .$$

Here the $\alpha_{n\sigma}$ are growth rates and the $\theta_{\sigma\nu\rho n}$ are saturation coefficients, which depend on the mode structure and

the gyromonotron operating parameters.[27] Upon substitution of Eq. (7) into Eq. (5) it is seen that the mode coupling occurs through both the mode phases and amplitudes. If the intermodal frequency separation is on the order of the separation between the drive signal and the driven mode, one might expect a complicated behavior which could be chaotic for a large enough drive signal or low enough cavity quality factors Q_0. We will focus attention on the simpler case of

$$\frac{2\pi}{\omega_d-\omega_n} \gg \frac{2\pi}{\omega_n-\omega_{n'}} .$$

Here we have two distinct time scales, one the fast beating between the drive signal and modes other than the nth, and the other the slow beating between the drive signal and the nth mode. In the case where the frequency separation between the modes is much larger than the cavity-mode linewidth, Eq. (5) may be averaged over the fast intermodal phase beating time scale.[26] Assuming furthermore that the difference in mode spacing is greater than the cavity linewidth of the nth mode ($2\omega_n-\omega_{n+1}-\omega_{n-1}>\omega_n/Q_0$) the phase equation becomes independent of the other mode phases,

$$\frac{d}{dt}\Psi_n+\frac{1}{2}\left[\omega_n+\frac{\omega_n}{Q_0^{nn}}-\frac{\omega_n^{0^2}}{\omega_n}\right] +\tfrac{1}{2}\,\mathrm{Re}\left[\alpha_{nn}+A_n^2\theta_{nnnn}+2\sum_{n'\neq n}A_{n'}^2\theta_{nnn'n'}\right] =-\frac{\omega_n}{2}\mathrm{Re}(\chi_{P_n}) . \quad (8)$$

Now the amplitude of the nth mode in the phase-locked state is assumed to be only slightly perturbed from its free-running value: $A_n=A_{\mathrm{osc}_n}+\delta A_n$. Because ω_n is the free-running steady-state frequency and the nonlinearity is weak ($\delta A_n\theta_n$ is second order), it is clear that the second two terms on the left-hand side of Eq. (8) cancel to first order. The gyromonotron is phase locked when the driven oscillation frequency equals that of the drive signal $\omega_d=\omega_n+\dot{\Psi}_n$, where for small premodulations the phase varies linearly, $\Psi_n(t)=\delta\omega_n t+\zeta$. Using these conditions and Eqs. (6) and (8) the locking bandwidth, maximized with respect to phase angle ζ, is

$$|\delta\omega_n|=\frac{\omega_n^0}{2}|\chi_{P_n}|=\left|\frac{\dfrac{\omega_d}{2\pi}\displaystyle\int_0^{2\pi/\omega_d}dt\int_V d^3r\,\mathbf{J}_{\mathrm{PM}}(\mathbf{r},t)\cdot\mathbf{e}_n^*(\mathbf{r})e^{-i\omega_d t}}{\epsilon_0\displaystyle\int_V d^3r\,\mathbf{E}_{\mathrm{osc}}(\mathbf{r})\cdot\mathbf{e}_n^*(\mathbf{r})}\right| , \quad (9)$$

where $\mathbf{E}_{\mathrm{osc}}(\mathbf{r})$ is the spacially dependent part of the free-running oscillator electric field. The electronic susceptibility χ_{P_n} is determined from the solution to the single-particle equations of motion.

2. *Calculation of the premodulated current density*

The experiments to be modeled employ prebunching configurations with two or three TE_{101} mode rectangular cavities separated by drift sections cutoff to the radiation (see Fig. 1 for a schematic). The theory, however, will be valid for any number of prebunching cavities of circular cross section. The results for the rectangular TE_{10} system are related to those of the TE_{11} cylindrical case in a simple way.[13] The cavity interaction can be approximated by considering the coupling of thin annular electron beam with the cavity mode at the fundamental cyclotron harmonic. The calculation of the prebunched current density makes use of a gyroklystron theory[13] which has been modified to allow for small linear tapers in the axial static-magnetic-field profile (see Appendix). These tapers are necessary in the theory since magnetic-field detuning was used to prevent multiple-cavity oscillation in the experiment. Since the bandwidth of the prebunching section is increased with magnetic tapers it is expected that the locking width also increases. Theoretical predictions of locking bandwidth are compared with experiment for cases with one and two prebunching cavities.

The electron beam geometry is shown in Fig. 2. The electron guiding centers are uniformly dispersed about the large circle of radius R_0 (guiding center coordinates are R_0,θ_0). No radial spread in guiding center is considered. This beam geometry is close to that generated by a MIG gun. The relativistic electron cyclotron frequency is given by Ω. The cavity wall radius is r_w, and the transverse cavity coordinates are r and θ. The parti-

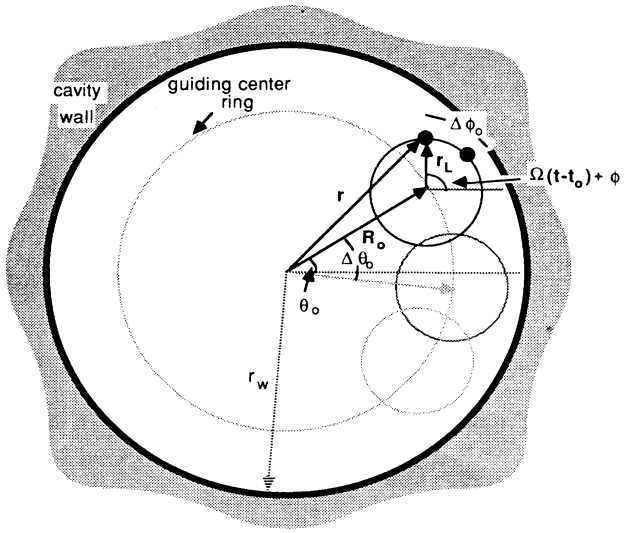

FIG. 2. Geometry of electron beam in cavity with guiding center R_0 and Larmor radius r_L. $\Delta\theta_0$ and $\Delta\phi_0$ are the increments used in calculation of the transverse current density. The cavity radial dimension is r_w.

cle dynamics are represented in the slow-time-scale formulation (variations in electron motion from the zeroth-order pure cyclotron motion are calculated) and the fields in cavities between the input cavity and the oscillator are calculated using a Green's function approach.[13] The electron equations of motion in a cavity supporting a TE mode are[28]

$$\frac{dp_\perp}{dt} = -F_x \sin(\omega t - \Lambda) + F_y \cos(\omega t - \Lambda) , \tag{10a}$$

$$p_\perp \frac{d\Lambda}{dt} = \left[\omega - \frac{\Omega_a \gamma_0}{\gamma}\right] p_\perp + F_x \cos(\omega t - \Lambda) + F_y \sin(\omega t - \Lambda) - e p_\perp \frac{\delta B_z}{\gamma m_e} , \tag{10b}$$

$$\frac{dp_z}{dt} = \frac{e}{\gamma m_e} p_\perp \delta B_r [\sin(\omega t - \Lambda)\sin\theta + \cos(\omega t - \Lambda)\cos\theta] , \tag{10c}$$

where the slowly varying phase $\Lambda = \omega t - \Omega_a (t - t_0) - \phi$, ω is the rf field frequency, t_0 is the entrance time of the electron into the cavity, γ is the relativistic factor, and F_x and F_y are defined by

$$\begin{aligned} F_x &= -e(E_r \cos\theta - E_\theta \sin\theta) + e p_z \frac{\delta B_r}{\gamma m_e} \sin\theta , \\ F_y &= -e(E_\theta \cos\theta + E_r \sin\theta) - e p_z \frac{\delta B_r}{\gamma m_e} \cos\theta . \end{aligned} \tag{11}$$

Here E_θ and E_r are components of the rf electric field. The electron rest mass and charge are given by m_e and $-e$, respectively. The equations of motion have been written to include the effect of small linear tapers in the static magnetic field. The magnetic field remains curl free and is written,

$$\mathbf{B} = \mathbf{B}_a + \delta\mathbf{B} , \tag{12}$$

where

$$\delta B_z = (z - z_{\rm av}) \left.\frac{dB}{dz}\right|_{z = z_{\rm av}}$$

and

$$\delta B_r = -\frac{r}{2} \left.\frac{dB}{dz}\right|_{z = z_{\rm av}}$$

and the subscript a indicates that the average value of the z component of the magnetic field (in a given cavity or drift section) is to be used in the subscripted quantity. The position $z_{\rm av}$ is that at which $B_z = B_a$. The subscript 0 in Eqs. (10) indicates the initial value (at the entrance to first cavity) and p_z and $p_\perp$ are the axial and perpendicular momenta, respectively. The slow-time-scale variables are related to the original momenta by

$$p_x + i p_y = i p_\perp e^{i[\Omega_a (t - t_0) + \phi]} .$$

For a TE_{ml} circular mode, the cavity electric field is

$$\mathbf{E} = \mathrm{Re}\left\{ C_{ml} \left[k_{ml} J'_m(k_{ml} r)\hat{\boldsymbol{\theta}} + \frac{im}{r} J_m(k_{ml} r)\hat{\mathbf{r}} \right] F(z) e^{i(\omega t - m\theta)} \right\} \tag{13}$$

which has right-handed circular polarization. Here $m = m_k$ and $l = l_k$ in the kth cavity. The transverse wave number k_{ml} is defined by

$$k_{ml} = \frac{x_{ml}}{r_w} ,$$

where x_{ml} is the lth zero of $J'_m(x)$. The normalization constant is

$$C_{ml} = \frac{1}{[\pi (x_{ml}^2 - m^2)]^{1/2} J_m(x_{ml})} .$$

Expanding the electric field about the electron guiding center and retaining only the slowly varying components at the fundamental cyclotron harmonic (and assuming $k_{ml} r_L \ll 1$, where r_L is the electron Larmor radius) the equations of motion inside a cavity can be compactly written (see Appendix)

$$\left[\frac{d}{dt} + i \left[(\omega - \Omega_a) - \frac{e\delta B_z}{\gamma m_e} + i \frac{\delta B_z v_z}{2|\mathbf{B}_a|(z - z_{\rm av})} \right] \right] p = -\tfrac{1}{2} e k_{ml} C_{ml} J_{m-1}(k_{ml} R_0) F(z) e^{-i[(m-1)\theta_0]} , \tag{14}$$

where the complex momentum is defined, $p = p_\perp e^{-i\Lambda}$. From these equations of motion the electron momenta are found as a function of the initial coordinates $(\phi_0, \theta_0, t_0, \mathbf{v}_0)$ and the time t. For reasonable electron densities ($\sim 10^5$ cm^{-3} in our case), the current density can be found by integrating over the electron initial conditions,

$$\mathbf{J}_{\rm PM}(\mathbf{r}, t) = \frac{-I_0}{m_e (2\pi)^2} \int_{\mathbf{v}} f(\mathbf{v}_0) \int_{t_0 = -\infty}^{\infty} \int_{\theta_0 = 0}^{2\pi} \int_{\phi_0 = 0}^{2\pi} \times \delta(\mathbf{r} - \mathbf{r}_{\rm orbit}) \frac{\mathbf{p}_\perp}{\gamma} d\phi_0 \, d\theta_0 \, dt_0 \, d^3\mathbf{v}_0 . \tag{15}$$

Here $\mathbf{r}_{\rm orbit}$ is the electron trajectory, I_0 is the dc beam current, and the quantities $\mathbf{r}_{\rm orbit}$, $\mathbf{p}_\perp$, and γ are functions of the variables t, ϕ_0, θ_0, t_0, and $\mathbf{v}_0$.

3. *Multiple-cavity phase-locking results*

Equation (15) is the proper expression for the transverse current in the gyromonotron to be used in Eq. (9). The potential, from which the circular TE_{ml} mode cavity eigenfunctions in Eq. (9) are calculated, is

$$\psi_{ml} = C_{ml} J_m(k_{ml} r) e^{-im\theta} .$$

The integration over the cavity cross section in Eq. (9) is done first, then the time-dependent unit vector $\hat{\boldsymbol{\phi}}$ is introduced into the electron momentum,

$$\mathbf{p}_\perp = p_\perp \hat{\boldsymbol{\phi}} = p_\perp \, \mathrm{Re}[e^{i[\Omega_{\rm osc}(t - t_0) + \phi]} (i\hat{\mathbf{x}} + \hat{\mathbf{y}})] . \tag{16}$$

The slow-time-scale formalism is introduced as the electric field is expanded about the electron orbits (all time scales more rapid than $\omega-\Omega_{\rm osc}$ are averaged away). Again the subscript osc denotes the value in the oscillator cavity. It has been shown that the limits on the integrations over t and t_0 may be interchanged.[29] The integration over time now merely replaces the variable t with a function of z because of the δ function from the electron density. The final result for the phase-locking frequency band is

$$|\delta\omega|=\frac{I_0 C_{ml} k_{ml} J_{m-1}(k_{ml}R_0)}{2m_e A_{\rm osc}\epsilon_0}\left|\int_0^L\left\langle\frac{p(z,\phi_0,\theta_0,t_0,\mathbf{v}_0)}{\gamma(z,\phi_0,\theta_0,t_0,\mathbf{v}_0)}\frac{e^{i(m-1)\theta_0}}{v_{z_{\rm osc}}}\right\rangle f_q^*(z)dz\right| , \tag{17}$$

where the average has been denoted

$$\langle N\rangle=\int_{\rm v} f(\mathbf{v}_0)\frac{\omega_d}{2\pi}\int_{t_0=0}^{2\pi/\omega_d}\frac{1}{2\pi}\int_{\theta_0=0}^{2\pi}\frac{1}{2\pi}\int_{\phi_0=0}^{2\pi}N\,d\phi_0\,d\theta_0\,dt_0\,d^3\mathbf{v}_0 .$$

$A_{\rm osc}$ is the free-running gyromonotron amplitude (mks units of $\mathrm{V\,m^{1/2}}$) and p, the complex momentum of Eq. (14), has again been used. All quantities depending on the eigenvalues m, l, and q are evaluated using the mode in the oscillator cavity. The solution for the particle dynamics through any number of prebunching cavities separated by drift regions in a uniform magnetic field is given in Ref. 13. Thus our nomenclature and method of solution are consistent with that source. An initial momentum of $p_{\perp_0}=\gamma_0 m v_{\perp_0}$ is used. The electric field in all prebunching cavities but the first is found by a self-consistent solution to the coupled momentum and wave equations. The electric field in the first cavity is generated solely by the external rf drive signal.

The individual cavities and drift tubes are defined as *sections* of the device. A *stage* in the device is defined as a prebunching cavity plus the following drift tube. The physical parameters in the problem are labeled if they are either section or stage dependent. In general, all quantities depending on the static magnetic field are section dependent while those dependent on the cavity rf electric fields are stage dependent. For example, the entrance position coordinate of the kth cavity is written as a sum over all previous stages

$$z_k=\sum_{j=1}^{2k-2}L_j ,$$

where L_j is the length of the jth section, numbered consecutively from the electron-gun end of the device. Thus the subscript on z indicates the kth stage while that on L indicate the jth section. It is annotated, wherever possible, in the following whether a given parameter is subscripted by stage or section. A normalization scheme is used to keep the radiation wavelength arbitrary.[13] Lengths are normalized to the radiation wavelength, velocity to the speed of light and energy to the rest energy of the electron. Other quantities are normalized consistently (see Appendix).

For the general case of phase locking using $N+1$ cavities (N prebunching cavities), we first calculate the transverse momentum at the entrance of the final cavity. This is done in the Appendix. The electron momentum in the oscillator cavity [$(N+1)$st cavity] is found using the calculated electron energy change through the first N cavities [see Eq. (A13) for energy change expression]. This momentum is now used to calculate the averaged quantity in Eq. (17). Using the relation $\delta\gamma=\bar{p}_{\perp_0}\delta\bar{p}_\perp/\gamma_0$, the averaged quantity can be written (to first order in $\delta\gamma/\gamma_0,\delta\bar{p}_\perp/\bar{p}_{\perp_0}$, and the ratio of the electron energy loss per rf cycle in the input rf field to the rest energy of the electron) as

$$\begin{aligned}\left\langle\frac{\bar{p}(\bar{z}_{N+1}+\bar{z})}{\gamma}e^{i(m-1)\theta_0}\right\rangle_{\theta_0,\phi_0,t_0}&=i\bar{p}_{\perp_0}\left[1-\frac{\bar{p}_{\perp_0}^2}{\gamma_0^2}\right]\exp\left[-i\sum_{j=1}^{2N}M_j\right]\bar{E}_1\\&\times\prod_{j=1}^{2N}h_j(A_1e^{-i\Delta^0_{2N+1}\bar{z}}+A_2\bar{z}e^{-i\Delta^0_{2N+1}\bar{z}}) ,\end{aligned} \tag{18}$$

where

$$\begin{aligned}A_1=&\frac{1}{2}\sum_{j=1}^{N}\sum_{k=j}^{N}\frac{x_{jk}}{\bar{E}_1}e^{i\sigma_{jk}}\delta_{m_j,m_{\rm osc}}\\&+i\sum_{j=1}^{N}\frac{\langle\beta_{2j-1}\rangle_{v_{z_0}}}{\beta_{2j-1}}\frac{R_j}{\bar{p}_{\perp_0}}\frac{\bar{E}_j}{\bar{E}_1}\\&\times\delta_{m_j,m_{\rm osc}}\frac{\prod_{k=2j-1}^{2N}h_k}{\prod_{k=1}^{2N}h_k} ,\end{aligned}$$

and

$$\begin{aligned}A_2=&\frac{1}{2}\frac{\bar{\omega}\bar{p}_{\perp_0}}{\beta_{2N+1}\gamma_0^2}\\&\times\sum_{j=1}^{N}\frac{\langle\beta_{2j-1}\rangle_{v_{z_0}}}{\beta_{2j-1}}R_j\frac{\bar{E}_j}{\bar{E}_1}\delta_{m_j,m_{\rm osc}}\prod_{k=1}^{2j-2}h_k .\end{aligned} \tag{19}$$

Here the relative phase change through the jth section, due to the variable electron Larmor frequency, between the electron beam wave and the rf field is given by

$$M_j=\frac{\bar{\Omega}_j\beta_j\bar{L}_j\gamma_0^2}{3\bar{p}_{\perp_0}^2 f_j}[(2+f_j)\sqrt{1-f_j}-(2-f_j)\sqrt{1+f_j}]$$
$$+\frac{(\bar{\omega}-\bar{\Omega}_j)\bar{L}_j}{\beta_j f_j}(\sqrt{1+f_j}-\sqrt{1-f_j})\ , \tag{20}$$

where the cyclotron frequency Ω and the ratio of axial electron velocity to the speed of light in vacuum β are labeled by section. Here f_j is proportional to the magnetic field gradient in section j,

$$f_j=\frac{\bar{p}_{\perp_0}^2}{2|\bar{\mathbf{B}}_0|\gamma_0^2\beta_j^2}\frac{d|\bar{\mathbf{B}}|}{d\bar{z}}\bigg|_j\bar{L}_j\ .$$

The change in the magnitude of the perpendicular momentum in section j due to conservation of the electron magnetic moment is

$$h_j=\left[1+\frac{\frac{d|\bar{\mathbf{B}}|}{d\bar{z}}\Big|_j\bar{L}_j}{|\bar{\mathbf{B}}_0|+\frac{d|\bar{\mathbf{B}}|}{d\bar{z}}\Big|_{j-1}\bar{L}_{j-1}}\right]^{1/2}\ , \tag{21}$$

where $\mathbf{B}_0$ is the axial magnetic field at the start of the first cavity and the detuning factor between the rf frequency and the cyclotron frequency in the jth section is

$$\Delta_j^0=\frac{1}{\beta_j}\left[\bar{\omega}-\frac{\bar{\Omega}_j\gamma}{\gamma_0}\right]\ .$$

The "bunching parameters," representing the modulation of the electron beam due to interactions in the jth and kth stages are

$$X_{jj}=\frac{\bar{\omega}\bar{p}_{\perp_0}}{\gamma_0^2}\eta_j\frac{\langle\beta_{2j-1}\rangle_{v_{z_0}}}{\beta_{2j-1}}\left|\bar{E}_j\left[\frac{T_j}{\beta_{2j-1}}+\frac{R_j\bar{L}_{2j}}{\beta_{2j}}\right]\right|\ ,$$
$$X_{jk}=\frac{\bar{\omega}\bar{p}_{\perp_0}}{\gamma_0^2}\eta_k\frac{\langle\beta_{2j-1}\rangle_{v_{z_0}}}{\beta_{2j-1}}\left|\bar{E}_jR_j\left[\frac{\bar{L}_{2k-1}}{\beta_{2k-1}}+\frac{\bar{L}_{2k}}{\beta_{2k}}\right]\right|\ , \tag{22}$$
$$j<k$$

where in the jth stage

$$\eta_j=\begin{cases}\prod_{k=1}^{2j-2}h_k & \text{if } j>1\\ 1 & \text{if } j=1\ .\end{cases}$$

The bunching parameters are written in terms of the stage-dependent quantities $\bar{E}$, T, and R which will be defined presently. The phase factors σ_{jk} (stage dependent) are

$$\sigma_{11}=\arg\left[\bar{E}_1\left[\frac{T_1}{\beta_1}+R_1\frac{\bar{L}_2}{\beta_2}\right]\right]\ ,$$
$$\sigma_{jj}=\arg\left[\bar{E}_j\left[\frac{T_j}{\beta_{2j-1}}+R_j\frac{\bar{L}_{2j}}{\beta_{2j}}\right]\right]\quad\text{for } j>1\ , \tag{23}$$
$$\sigma_{jk}=\arg(\bar{E}_jR_j)\quad\text{for } k>1\ .$$

The normalized electric field strength in the jth cavity is

$$\bar{E}_j=\tfrac{1}{2}F_j\frac{e}{\langle\beta_{2j-1}\rangle_{v_{z_0}}m_ec^2}$$
$$\times C_{m_jl_j}\bar{k}_{m_jl_j}J_{m_j-1}(k_{m_jl_j}R_0)\ , \tag{24}$$

where the modal indices m and l are subscripted by stage. The beam-generated electric field in the jth cavity is found in terms of the electric field in previous cavities,

$$\bar{E}_j=-i\bar{I}_j\left\langle\bar{p}(\bar{z}_j)\frac{f(v_{z_0})}{\gamma}e^{i(m_j-1)\theta_0}\right\rangle\exp\left[i\sum_{k=1}^{2j-2}M_k\right]\ ,$$

$$\bar{E}_j=\left\langle\bar{p}_{\perp_0}\left[1-\frac{\bar{p}_{\perp_0}^2}{\gamma_0^2}\right]\bar{I}_j\prod_{k=1}^{2j-2}h_k\left[\tfrac{1}{2}\sum_{s=1}^{j-1}\sum_{k=2}^{j-1}x_{sk}e^{i\sigma_{sk}}\delta_{m_j,m_s}+i\sum_{k=1}^{j-1}\frac{\langle\beta_{2k-1}\rangle_{v_{z_0}}}{\beta_{2k-1}}\frac{\bar{E}_k}{\bar{p}_{\perp_0}}R_k\frac{\prod_{n=2k-1}^{2j-2}h_n}{\prod_{n=1}^{2j-2}h_n}\delta_{m_k,m_j}\right]\right\rangle_{v_{z_0}}\ , \tag{25}$$

where the normalized beam current is

$$\bar{I}_j=\frac{eI_0\bar{\omega}_0}{2\epsilon_0m_ec^3\langle\beta_j\rangle^2}\bar{k}_{m_jn_j}^2C_{m_jn_j}^2J_{m_j-1}^2(k_{m_jn_j}R_0)\ . \tag{26}$$

The constants R_j and T_j have the same definitions as in Ref. 13 and are given in Eqs. (A8), (A9), (A11), and (A12) for convenience. The Kronecker δ functions ($\delta_{m,n}$) in Eq. (19) originate in the averages over the guiding center coordinate θ_0. The result is that if the azimuthal mode index in any of the prebunching cavities is not the same as in the oscillator, then the bunching term from that cavity does not contribute. For maximum performance one therefore requires that all the cavities have the same azimuthal mode index.

The locking width for a system with N prebunching cavities is obtained by using Eq. (18) in Eq. (17). The axial electric field eigenfunction is assumed to be sinusoidal in the oscillator cavity (start of $N+1$st stage of device),

$$f_{q_{N+1}}(\bar{z})=\left[\frac{2}{\bar{L}_{2N-1}}\right]^{1/2}\sin[\bar{k}_{z_{N+1}}(\bar{L}_{2N-1}-\bar{z})]\ ,$$

where the axial wave number $\bar{k}_{z_{N+1}}\approx q\pi/\bar{L}_{2N-1}$. The expression for the locking width is

$$|\delta\bar{\omega}_{\max}|=\frac{\bar{I}_{N+1}}{\bar{L}_{2N+1}\bar{\omega}_0}\frac{\bar{E}_1}{\bar{E}^{\,\mathrm{osc}}_{N+1}}\prod_{k=1}^{2N}h_k\left|\left\langle\bar{p}_{\perp_0}\left[1-\frac{\bar{p}^2_{\perp_0}}{\gamma_0^2}\right]\frac{\langle\beta_{2N+1}\rangle_{v_{z_0}}}{\beta_{2N+1}}(A_1\bar{R}_{N+1}+A_2P_{N+1})\right\rangle_{v_{z_0}}\right|\ , \tag{27}$$

where A_1 and A_2 have been defined in Eq. (19) and

$$\bar{R}_{N+1}=\int_{\bar{z}=0}^{\bar{L}_{2N+1}}\sin[\bar{k}_{z_{N+1}}(\bar{L}_{2N+1}-\bar{z})]e^{-i\Delta^0_{2N+1}\bar{z}}d\bar{z}$$

is the complex conjugate of R_1 with the substitutions $\bar{L}_1\rightarrow\bar{L}_{2N+1}$ and $\bar{k}_{z_1}\rightarrow\bar{k}_{z_{N+1}}$. The definition of P_j is

$$P_j=\int_{\bar{z}=0}^{\bar{L}_{2j-1}}\sin[\bar{k}_{z_j}(\bar{L}_{2j-1}-\bar{z})]\bar{z}e^{-i\Delta^0_{2j-1}\bar{z}}d\bar{z}\ ,$$

which evaluates to

$$P_j=\frac{1}{\bar{k}^{\,2}_{z_j}-\Delta_k^{0^2}}\left[\bar{k}_{z_j}\bar{L}_k\cos(\Delta_k^0\bar{L}_k)+\frac{2\bar{k}_{z_j}\Delta_k^0\sin(\Delta_k^0\bar{L}_k)-(\bar{k}^{\,2}_{z_j}+\Delta_k^{0^2})\sin(\bar{k}_{z_j}\bar{L}_k)}{\bar{k}^{\,2}_{z_j}-\Delta_k^{0^2}}\right]$$
$$+\frac{i}{\bar{k}^2_{z_j}-\Delta_k^{0^2}}\left[\frac{2\bar{k}_{z_j}\Delta_k^0[\cos(\Delta_k^0\bar{L}_k)-\cos(\bar{k}_{z_j}\bar{L}_k)]}{\bar{k}^{\,2}_{z_j}-\Delta_k^{0^2}}-\bar{k}_{z_j}\bar{L}_k\sin(\Delta_k^0\bar{L}_k)\right]\ ,$$

where the subscript $k=2j-1$. The normalized oscillator amplitude is given by

$$\bar{E}^{\,\mathrm{osc}}_{N+1}=\tfrac{1}{2}A_{\mathrm{osc}}\left[\frac{2}{\bar{L}_{2N-1}}\right]^{1/2}\frac{e}{\langle\beta_{2N-1}\rangle_{v_{z_0}}m_ec^2}C_{m_{N+1}l_{N+1}}\bar{k}_{m_{N+1}l_{N+1}}J_{m_{N+1}-1}(k_{m_{N+1}l_{N+1}}R_0)\ .$$

The average over axial velocity spread in the jth cavity can be written in terms of an average over initial axial velocity spread by using Eq. (A5) obtained from conservation of electron magnetic moment. The relation is

$$\langle\beta_{z_j}\rangle_{v_{z_0}}=\left\langle\left[\beta^2_{z_0}\left[1+\sum_{k=1}^{j-1}\frac{L_k}{|\mathbf{B}_0|}\frac{d|\mathbf{B}|}{dz}\bigg|_k\right]-\left[1-\frac{1}{\gamma_0^2}\right]\sum_{k=1}^{j-1}\frac{L_k}{|\mathbf{B}_0|}\frac{d|\mathbf{B}|}{dz}\bigg|_k\right]^{1/2}\right\rangle_{v_{z_0}}\ .$$

The average over velocity spread is done numerically. The distribution function $f(\mathbf{v}_0)$ is assumed to be Gaussian in v_z and the beam is assumed to be monoenergetic,

$$f(\mathbf{v}_0)\sim\exp\left[-\frac{(v_{z_0}-\langle v_{z_0}\rangle)^2}{2(\Delta v_z)^2}\right]\delta\left[v^2_{\perp_0}+v^2_{z_0}-c^2\left[1-\frac{1}{\gamma_0^2}\right]\right]\ .$$

For a system of two rectangular TE_{101} mode cavities (modeling the experimental system) the general relation for the phase-locking limits Eq. (27) reduces to

$$|\delta\bar{\omega}_{\mathrm{two}}|=\frac{\bar{I}_2}{\bar{L}_3\bar{\omega}_0}\frac{\bar{E}_1}{\bar{E}^{\,\mathrm{osc}}_2}\left|\left\langle\bar{p}_{\perp_0}\left[1-\frac{\bar{p}^2_{\perp_0}}{\gamma_0^2}\right]\frac{\langle\beta_1\rangle_{v_{z_0}}}{\beta_1}\frac{\langle\beta_3\rangle_{v_{z_0}}}{\beta_3}\right.\right.$$
$$\left.\left.\times\left\{\left[\frac{1}{2}\frac{\bar{\omega}\bar{p}_{\perp_0}}{\gamma_0^2}\left[\frac{T_1}{\beta_1}+\frac{R_1\bar{L}_2}{\beta_2}\right]+i\frac{R_1}{\bar{p}_{\perp_0}}\right]\bar{R}_1+\frac{1}{2}\frac{\bar{\omega}\bar{p}_{\perp_0}}{\gamma_0^2}\frac{R_1}{\beta_3}P_2(\bar{L}_3)\right\}\right\rangle_{v_{z_0}}\right|\delta_{m_2,m_1}\prod_{k=1}^{2}h_k\ , \tag{28}$$

where the relations

$$k_{11} \rightarrow \frac{\pi}{L_x} \text{ and } C_{11}k_{11} \rightarrow \left[\frac{2}{L_x L_y}\right]^{1/2}$$

are used to transform the expressions from the TE_{11} circular mode to TE_{10} rectangular. Similar results follow for the three-cavity device.

It can be seen that the phase-locking frequency band given by Eq. (27) is of the same form as the Adler relation, Eq. (1). The drive and oscillator amplitudes are given by $\bar{E}_1$ and $\bar{E}^{\,\mathrm{osc}}_{N+1}$ instead of the powers P_d and P_0. The important difference is that in Eq. (27) the drive amplitude is multiplied by a gain factor given by the quantity in the absolute value. It is to be noted that this gain factor is not identical with that of an $N+1$ cavity gyroklystron amplifier. This is because the prebunched current does not excite the field in the final (oscillator) cavity.

Since both sides of Eq. (27) depend on the external signal frequency, the locking band must be found using an iterative technique. The strong frequency dependence of the gain factor often results in a locking band which is not symmetric about the free-running frequency of the oscillator. This phenomenon will be seen later in the experimental results.

C. Priming of the gyromonotron

Priming, or phase initiation of a pulsed oscillator by a cw driver, was observed experimentally and analyzed theoretically in the early work on controlling the phase of magnetrons.[21,30,31] There has also been recent work done on solid-state oscillators[32–34] and magnetrons.[35–37] The pulsed oscillation, though self-excited, grows from an initial condition of random noise. This results in total phase incoherence between one oscillator pulse and the next. The introduction of a stable, cw external signal during the oscillation build up increases the amount of interpulse phase coherence. The amount of start-up phase jitter in the presence of this external priming signal can be estimated using a lumped circuit representation of the oscillator. Before the oscillation starts, small variations in electron current density excite fluctuating voltages (noise) in the oscillator cavity. Though the noise is wideband, the presence of the cavity filters all but a narrow band of frequencies within a range determined by the cavity Q factor. Thus the noise frequency is reasonably close to that of the injected signal though its phase varies randomly. The noise amplitude varies statistically about some mean. The net voltage in the cavity is given by the vector sum of the injected signal and the noise signal (see Fig. 3). It is clear that the phase of the net voltage will vary over a smaller range as the amplitude ratio between the signal and noise becomes larger. The probability of start up at a given phase can be determined as a function of the rms signal-to-noise ratio once the statistical behavior of the noise amplitude is known. From the half-width of this probability distribution a root-mean-square deviation in start-up phase can be found. This value can be compared directly with experimental results. This comparison, using some measurements of gyromonotron preoscillation noise, are made in another work.[14] It should be emphasized that this priming phenomena does not control the frequency of the oscillator. A separate system, such as a phase-locked loop,[38] must be used if phase coherence is required throughout the pulse.

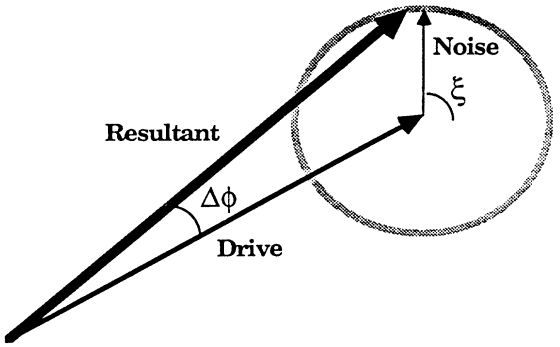

FIG. 3. Phasor diagram of voltage signals during priming of oscillation. Shaded circle indicates random-phase variation of the noise vector. Initial oscillation phase is constrained to $\pm\Delta\phi$ about that of the drive signal.

IV. EXPERIMENTAL RESULTS AND DISCUSSION

A. Direct-injection phase locking

It has been previously shown that a gyromonotron can be phase locked by the direct-injection method.[39] We verify those results by phase locking an oscillation in cavity no. 1. The plotted points in Fig. 4 show the drive power required to lock the cavity no. 1 oscillation at a given frequency separation between oscillator and driver. The gyromonotron is phase locked in the entire region between the two sets of points. The solid curves in the same figure show the phase-locking limits predicted from

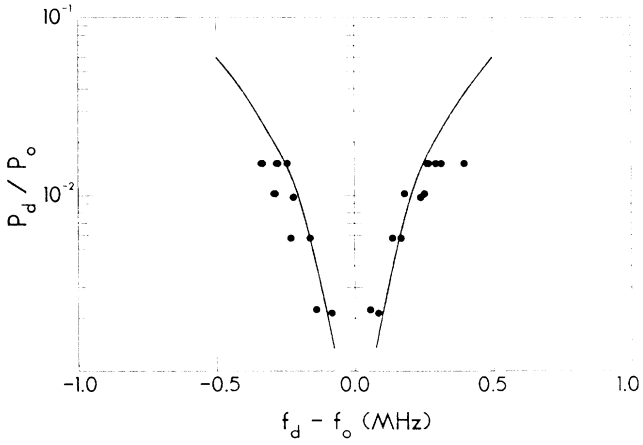

FIG. 4. Phase locking by direct injection of rf into cavity no. 1.

the time-independent solution [Eq. (1)] of Adler's equation. The agreement between the experimental results and theory is quite good for small drive power (the theory assumes that the drive power is small compared to the oscillator power). The oscillation strength in cavity no. 1 is on the order of 1 kW. Care is taken to assure good isolation between the driver system and the output radiation from cavity no. 1. Direct-injection locking, as a technique, is hampered by the fact that the drive radiation must be launched through the output line of the oscillator via a circulator. There is always the danger of locking or damaging the driver if adequate isolation from the oscillator is not present.

B. Phase locking by premodulation of the electron beam

The second cavity can be phase locked by applying the external drive signal to the first cavity and allowing the modulated electron beam to interact with the second cavity oscillation. The 30 dB isolation between the cavities prevents the input rf signal from leaking directly into the second cavity oscillator. Though the first two cavities are identical in construction it is possible to keep the input cavity quiescent by tuning the Doppler-shifted electron cyclotron frequency of the beam well above the cavity resonant frequency. This is done by raising the magnetic field in the first cavity and mechanically lowering the cold-cavity resonant frequency. Unfortunately in this condition the first cavity is not able to absorb radiation very well at the frequency at which the second cavity is oscillating. The results of this two-cavity locking system are shown in Fig. 5. The experimental resolution in frequency separation is $\sim \pm 0.1$ MHz. Here, once again, the locking bandwidth is shown for different drive-to-oscillator power ratios. It can be seen that the experimental locking width is considerably wider than predicted from the Adler relation, shown by the dashed curves. This difference can be understood as an intensification of electron beam modulation between the input and output cavities due to the same gain mechanism that operates in the gyroklystron amplifier (regenerative amplification in the first cavity and gain due to ballistic phase bunching of electrons in the drift section). Thus, by using a prebunching cavity, not only are problems of driver protection circumvented but the drive signal can be enhanced in transit to the gyromonotron. The steady-state locking angle is found to vary approximately between $\pm 90°$ as would be expected from Adler's theory.[20]

The solid curves in Fig. 5 are the predictions of the multicavity theory, Eq. (28), taking into account the tapered magnetic-field profile and assuming an α of 1.5 and a velocity spread of 5%. The nominal cavity tuning is 4.472 GHz. The free-oscillation power level is 1.3 kW, and the oscillation frequency is 4.482 GHz. The magnetic field is tapered upwards from the electron gun to the oscillator cavity, and a downward taper is used through the rest of the tube. The average magnetic field is 1.575 kG, and the tapers are $\sim 4\%$. The beam voltage is 29.8 kV, beam current 4.92 A, and the electron guiding center radius R_0 is 0.9 cm. In the regime of validity of the small-signal theory (for low drive powers) the theory agrees quite well with the experimental results. The asymmetry in the experimental points is partly a large-signal effect to be discussed later. The small-signal theory does, however, predict some asymmetry because the gain of the prebunching stage optimizes at a frequency below that of the free-running oscillation.

Figure 6 shows the further increase in locking bandwidth obtained by using two cavities to premodulate the beam. The third cavity is run as a free gyromonotron oscillator (20 kW output power) and the drive signal is injected into the first cavity. Note that the locking width predicted by the Adler relation in Fig. 6 is much larger than in Fig. 5 at a given power ratio due to the fact that Q_e for the third cavity is only 375. The three-cavity system allows locking at more than 15 dB below the Adler limit. The two-cavity gain in the amplifier mode is 10–20 dB, which accounts for this 15 dB improvement.

The results of the multicavity phase-locking theory (solid curves) are once again in good agreement with the experimental points. A beam voltage of 28.0 kV, beam current 5.74 A, an α of 1.0, and a 5% velocity spread are

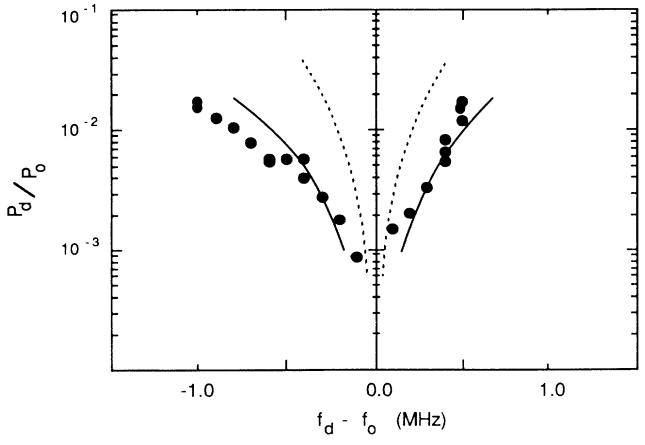

FIG. 5. Phase locking of cavity no. 2 gyromonotron by premodulating the beam in cavity no. 1.

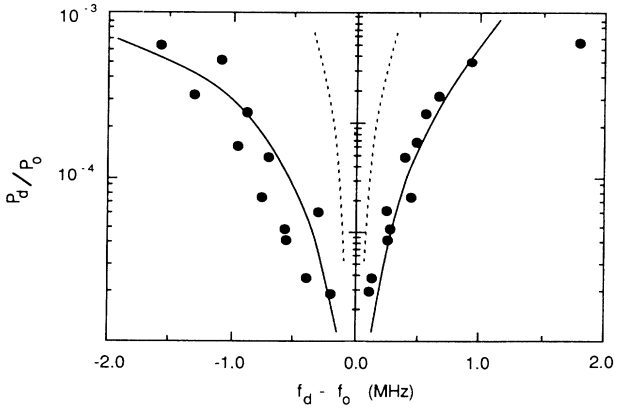

FIG. 6. Phase locking of cavity no. 3 gyromonotron using two cavities to premodulate the beam.

used in this calculation. The magnetic-field profile is of the same shape as for the two-cavity experiment except with an average of 1.547 kG. Note the strong asymmetry in the locking band at large drive-to-oscillator power ratios.

The code does not include susceptive beam loading effects on the coupling of the external signal to the cavity. We have found that the experimentally observed frequency of maximum gyroklystron amplifier gain is ~ 30 MHz higher than that predicted by the code. Thus this effect is introduced as a correction to the experimental frequencies when used in the code.

It is found in this experiment that the cavity resonant frequencies should be stagger tuned for most efficient phase-locked operation. This is due to the increased frequency pushing effect of the electron beam as the bunching process takes place. The frequency of maximum absorption of the first cavity is about 10 MHz higher than the cold cavity resonance while the maximum emission from the third cavity comes at 60 MHz above the cold resonance. To make these frequencies equal the resonant frequency of the third cavity is mechanically tuned downwards by ~ 50 MHz. The second cavity is tuned to a cold-resonant frequency approximately halfway between the other two.

In summary, the results indicate that a gyromonotron can be most effectively phase locked by introducing a modulated electron beam into the oscillator. The advantages over direct-injection locking include potential gain of the drive signal upon traversal of the drift sections and intermediate cavities and natural separation between the driving components and the cavity oscillator. This separation allows both protection of the driving components and more effective coupling of the drive signal onto the beam.

Another phase locking issue briefly investigated is that of phase locking by a large drive signal. Figure 7, where data is taken from a two-cavity experiment, shows extreme asymmetry and expanded locking width compared with the Adler prediction. The fact that the locking width may exceed the Adler prediction at large drive powers agrees qualitatively with gyromonotron direct-injection measurements in a previous experiment[39] and is understandable since Adler's result is based on a small-signal approximation. The asymmetry in locking width is due to two effects. The first is the previously mentioned dependence of the premodulation section gain on frequency, and the second is the effect of asynchronous quenching. If the frequency of maximum gyroklystron gain through the first drift section is lower than the second cavity oscillation frequency then the low-frequency drive signals appear larger at the second cavity, and there is a corresponding shift in the locking band (this effect is noted to a lesser degree in the small-signal cases as well). Note that the total locking width in Fig. 7 is limited to ~ 8 MHz which is the bandwidth of the first cavity. The second reason for the asymmetry in locking width is the presence of an entirely different phenomenon on the lower locking edge. It is observed that the process of unlocking is different on the upper and lower locking edges. The upper edge exhibits the normal sudden appearance of a large beat signal in the output of the mixer diagnostic as the oscillator unlocks. At the lower locking edge the beat signal which is present seems to "grow" from zero amplitude as the drive frequency is lowered. The curve shown on the left-hand side of Fig. 7 marks the frequencies at which this small beat signal first became visible. This growth in amplitude of the beat signal indicates that the free oscillation in the second cavity is being suppressed rather than locked by the drive signal along this lower "locking edge." The area where this suppression may be occurring is indicated by the dashed contour in Fig. 7. The transition from the phase-locking regime to that of asynchronous quenching can be experimentally determined from a rapid change in the steady-state relative phase between the oscillator and driver.[40] This experiment has not yet been done. Within the asynchronous quenching region the drive signal initiates an oscillation which competes with the self-excited oscillation in the second cavity. The brief explanation, given previously, indicated two types of quenching, passive and active. From the available data it is not possible to determine which type is in evidence in Fig. 7.

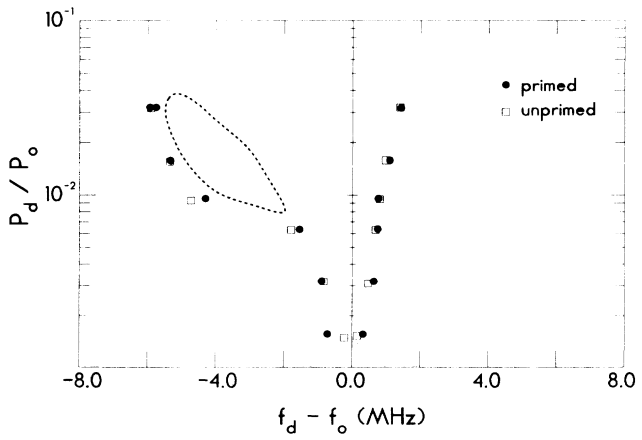

FIG. 7. Phase locking with large drive signal. Drive not present during oscillation buildup (unprimed), overlapped (primed), and estimated region of oscillation quenching (dash).

By pulsing the rf drive signal it is found that the locking frequency limits are independent of the turn-on sequence of driver and gyromonotron (see Fig. 7). The experimental points marked "primed" are those taken when the drive signal is introduced during the oscillation buildup (drive pulse overlaps front edge of oscillator pulse). The pulse-to-pulse phase coherence, however, is degraded if the drive signal is introduced after the buildup of the oscillation.

C. Priming of the gyromonotron

Here we include a brief description of experimental priming results with the aim of comparing them with those of phase locking. The details of these experiments appear elsewhere.[14] The most fundamental difference between priming and phase locking is that the latter occurs

abruptly as the system parameters are adjusted into the phase-locking regime. The priming effect is one of degree. The pulse-to-pulse phase control in a primed oscillator may be determined by measuring the rms phase variation between the oscillator and external signal. From Fig. 3 it is clear that one may have varying degrees of phase control in a primed oscillator depending on the size of the external signal. The external signal power required for significant phase control via priming is generally several orders of magnitude lower than that required for phase locking. For a primed oscillator, the degree of phase control diminishes both as the frequency separation between the driver and oscillator is increased and as the external drive power is decreased. This is similar to the phase-locked oscillator which must meet the criterion of the Adler relation. We have found that the bandwidth over which there is significant phase control in the primed case is on the order of the cavity no. 1 bandwidth (8 MHz). This is much larger than the bandwidth over which phase-locking takes place using similar drive power. The largest drawback of priming is that, unlike phase locking, there is no control over the oscillator frequency.

Due to the amplification through the first cavity and drift section, we have found that priming, like phase locking, can be achieved at much lower drive powers by using a premodulation section. One requires about three orders of magnitude less external signal power to achieve primed phase control equivalent to that of the direct-injection case. The bandwidth over which significant phase control (less than 5° phase variance from pulse to pulse) was realized was almost twice that of cavity no. 1.

D. Regimes of qualitatively different behavior

The term "gyromonotron" has been used exclusively when referring to the electron cyclotron maser device consisting of a single-cavity, self-excited oscillator. In discussing the more general behavior of the single-cavity maser we use the term ECRM, modified by either "oscillator" or "amplifier" to signify the class of operation. Here we make a short study of the different responses that the ECRM may have to an externally applied signal. The three regimes investigated are those of amplification, soft excitation, and hard excitation, using the terminology from the classical theory of nonlinear oscillations.[41] These regimes can be identified in different areas of the "oscillator plane" defined by the uniform axial magnetic field and the electron beam current, all other parameters being fixed. The qualitatively different features of these regimes will now be discussed.

1. Amplifier regime

Amplifier behavior can be seen in a single-cavity ECRM system when the beam current is below the start oscillation threshold and beam-cavity parameters are such that the beam provides negative loading. A signal injected through the cavity output will experience gain upon reflection from the ECRM amplifier. In a multiple-cavity system the same criterion applies except the input cavity provides positive loading. Figure 8

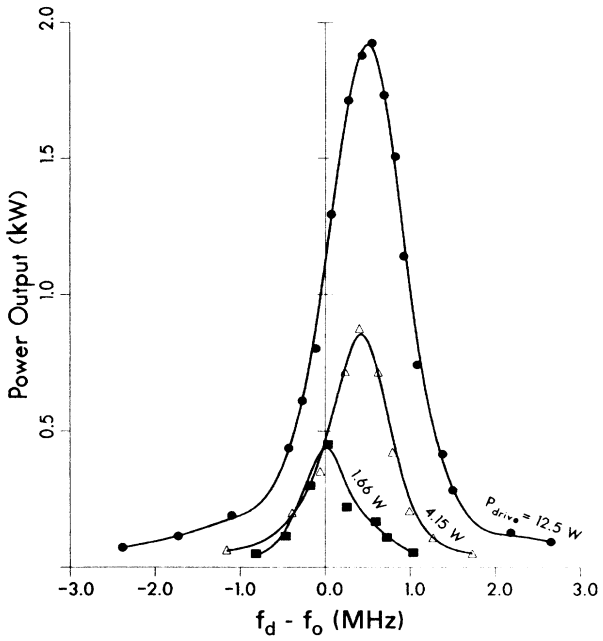

FIG. 8. ECRM amplifier amplitude-frequency response.

shows the typical amplitude-frequency response of an ECRM amplifier (three-cavity gyroklystron). The fact that the frequency corresponding to maximum gain is a function of drive power shows the effect of nonlinearity in the system. Features of the amplifier regime are that (1) there is output from the system only when the external signal is present, (2) the output is related in phase to the drive signal, (3) the output increases linearly with small drive powers and proceeds smoothly to a saturation regime which can be due to overbunching of electrons (in the multicavity case),[42] phase trapping, or energy depletion.[43]

2. Soft-excitation regime

The amplitude-frequency response of the soft-excitation regime is shown in Fig. 9, (free oscillation in cavity no. 1, drive applied to cavity no. 1). The first characteristic is that the oscillation is self-excited and grows spontaneously from noise. For drive powers (applied to the ECRM oscillator either by direct rf injection or premodulation of the electron beam) below a critical level (depending on the driver-oscillator frequency separation), the oscillation is autonomous. Above this critical power level the ECRM oscillation becomes phase locked; the oscillation frequency assumes that of the drive and becomes related in phase to the drive. There is some variation in the ECRM oscillator output power level with drive power inside of the locking band. In general, it is to be expected that the ECRM oscillator power could either increase or decrease inside the locking band depending on how close to saturation the oscillator is operating.

A simple way to visualize the phenomena of soft excitation (in the absence of an external signal) is to use the phase-space diagram shown in Fig. 10(a).[41] The two

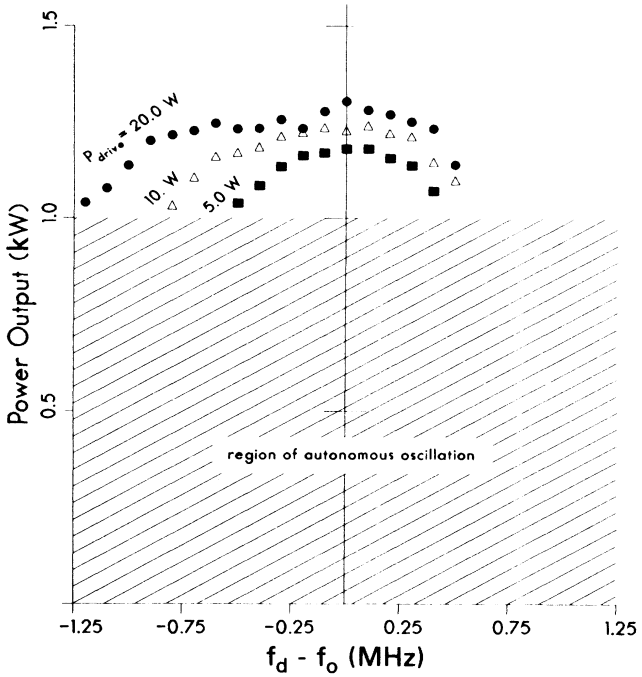

FIG. 9. Amplitude-frequency response for ECRM oscillator in soft-excitation regime.

coordinate axes are some conjugate variables characterizing the oscillation $(E, dE/dt)$ which may, for example, be related to the electric field amplitude and its time derivative. The system starts at some point on the phase plane, specified by the initial conditions, then proceeds along the trajectory along which it lies. In this case there are two equilibria, one at the origin and the other the limit cycle represented by the dashed line. Only the latter equilibrium is stable since trajectories wind towards the limit cycle from both directions (regions I and II). Thus the steady state is independent of initial conditions and the oscillation is self-excited since the point (0,0) is unstable.

Soft excitation can be determined experimentally by the way the oscillator system responds to a slowly varied

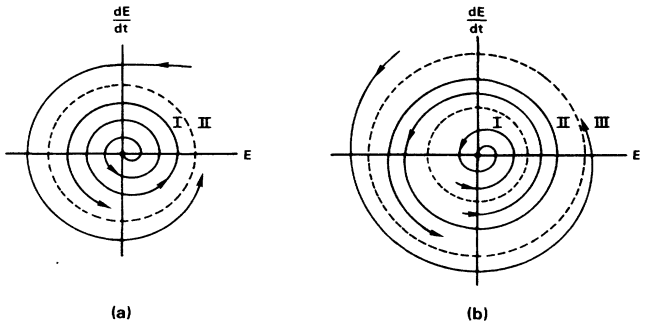

FIG. 10. Phase-space diagrams (a) soft excitation; (b) hard excitation.

oscillator parameter[44] (which in the ECRM oscillator could be the axial magnetic field, beam current, output load, etc.). If the nature of the oscillator is such that the amplitude changes continuously from zero as the parameter is varied then the oscillation is a case of soft excitation. This behavior is seen in the ECRM as the beam current, for example, is increased through the start oscillation current. Note that this test of soft excitation can be done in the steady state and does not examine the time-dependent features depicted in the phase plane example.

3. *Hard-excitation regime*

Hard excitation is the situation where, as in Fig. 10(b), the origin is a stable equilibrium. There are two limit cycles, one unstable and the other stable. If the initial condition of the oscillator is in either in regions II or III then the system moves to a new equilibrium. The new equilibrium is now a steady-state oscillation, shown by the outermost limit cycle. It can be seen that there is an amplitude threshold which the initial condition must exceed (large enough to reach region II) for the system of Fig. 10(b) to begin to oscillate. The final steady state, however, is insensitive to any other characteristics of the initial condition. The hard-excitation regime can be identified when a normally stable system is driven into a state of free oscillation by an external perturbation of arbitrary characteristics other than that it exceeds a given amplitude. An external signal, present during the course of the oscillation, can phase lock the oscillation in the hard-excitation regime just as in the soft.

Hard excitation also can be identified by slowly varying an otherwise static oscillator parameter. The oscillation amplitude will be observed to change discontinuously from a steady-state value.[44]

Figure 11 shows the experimentally observed phenomenon of hard excitation in the ECRM oscillator. The oscillation is in cavity no. 3, and the drive is applied to cavity no. 1. The drive signal is only present during the first 1 μsec of the high-voltage pulse across the electron gun [Fig. 11(c) shows the schronization]. Thus the drive signal provides an initial condition for the oscillator other than $(E=0, dE/dt=0)$. There is no oscillation present in the absence of the drive signal Fig. 11(a). For a drive signal of 286 mW, a stable oscillation is excited for the duration of the electron beam pulse [see Fig. 11(b)]. Unlike the bulk of the pulse, the pulse front edge is affected by the amplitude of the drive signal. No further change takes place in the bulk of the pulse as the drive amplitude or frequency are varied (within the cavity no. 1 bandwidth).

Another experiment reveals the temporal connection between the application of the drive signal and the initiation of the oscillation. As the drive pulse is moved later in the electron beam pulse it is found that the oscillation starts correspondingly later in time with respect to the start of the electron beam. In all cases it is found that the oscillation continues for the remainder of the electron beam pulse. Thus it is clear that it is the external signal which provides the starting condition for the hard excit-

ed oscillation.

A drive curve of the three-cavity device operating in the hard-excitation regime is shown in Fig. 12. There is weak amplification of the drive signal for small drive powers (the drive signal is applied over the entire electron beam pulse in this case). When a critical drive power is reached, the oscillation initiates and the output power increases dramatically. The phase discriminator reveals

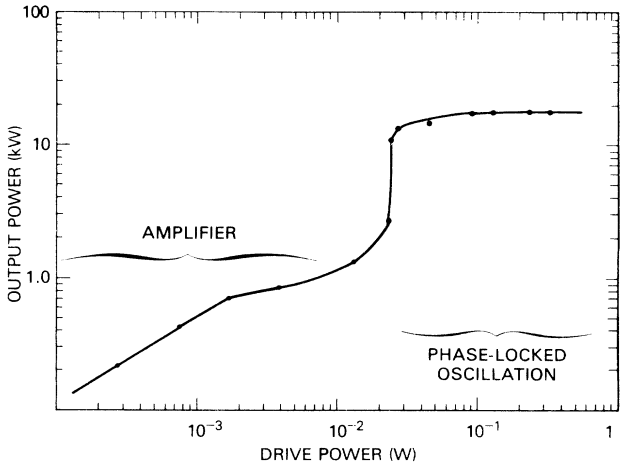

FIG. 12. Drive curve in hard-excitation regime for same oscillator parameters as Fig. 13; cw drive.

that the output of the device is phase locked to the drive throughout the drive curve. Thus the drive power which initiates the oscillation is enough to cause it to phase lock. There is no reason to assume that this would generally be the case. If the drive frequency were varied significantly from that of the oscillation, for example, there might still be initiation of the oscillation but no phase locking.

Figure 13 shows an example of the amplitude-frequency response in the hard-excitation regime. This data is again from a cavity no. 3 oscillation initiated by a

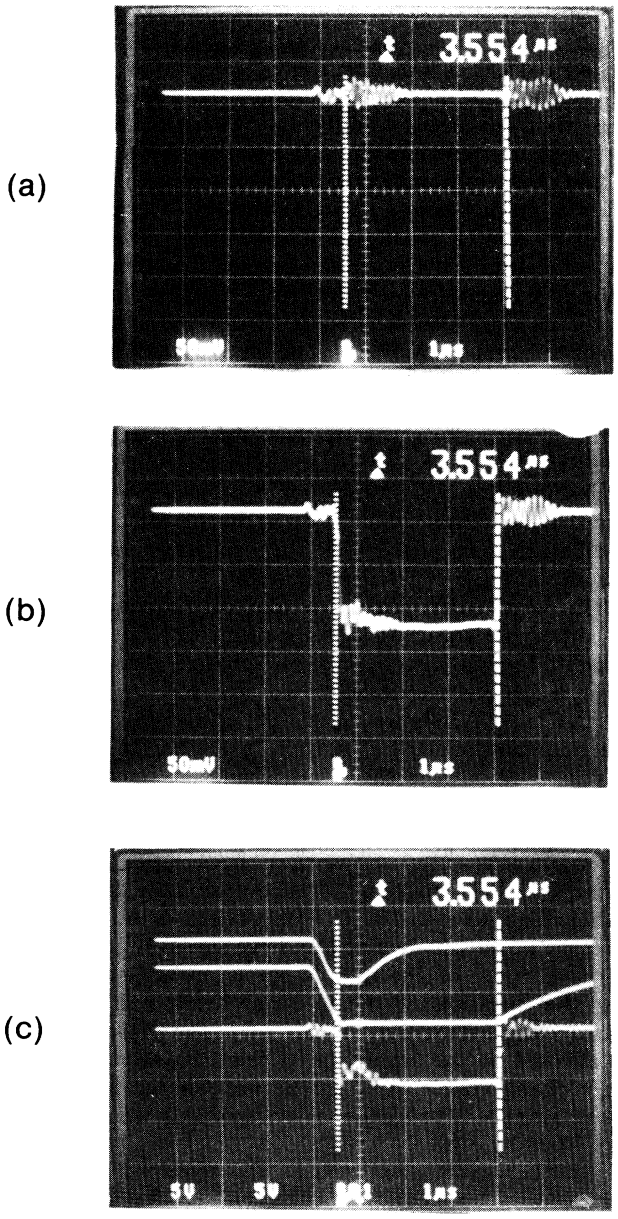

FIG. 11. Oscillographs of crystal diode traces monitoring ECRM oscillator output rf power in hard-excitation regime. (a) $P_d = 0$, no external signal applied; (b) $P_d = 286$ mW, excitation of 12.1 kW oscillation with drive frequency equal to oscillation frequency; (c) synchronization of (from top) drive rf pulse, electron-gun high-voltage pulse, and output rf oscillation.

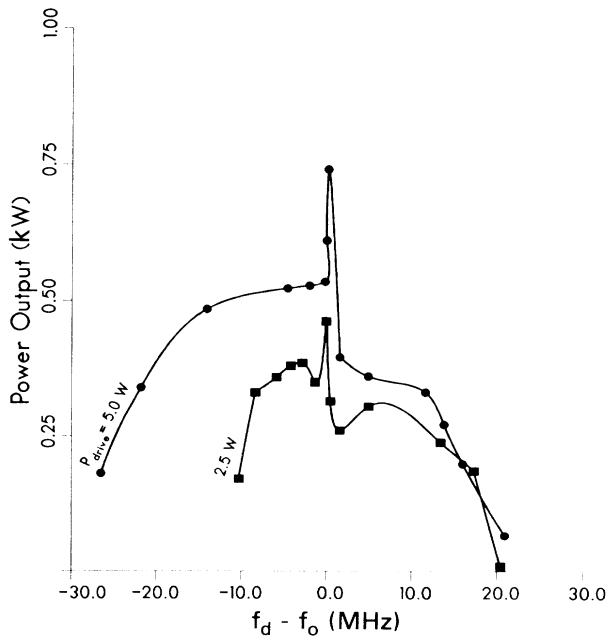

FIG. 13. Amplitude-frequency response for ECRM oscillator in hard-excitation regime.

drive signal applied to cavity no. 1. Note that the oscillation is excited by a wide range of drive frequencies. The oscillation frequency, however, is never affected by the drive signal except in the narrow region about $f_d - f_0 = 0$, where the ECRM oscillator becomes phase locked. In this experiment the drive signal is on throughout the oscillation pulse so that there is some dependence of the oscillator power on the drive power. If the ECRM oscillator cavity was long enough to produce a beam-wave saturation condition, then this power dependence probably would not be evident. If an amplifier is designed to operate in the hard-excitation regime, bandwidths cannot be expected beyond that over which the oscillation is phase locked. Figure 13 shows that this is a small fraction of the cavity bandwidth.

This method of accessing the hard-excitation regime may have application for electronic efficiency enhancement of gyromonotrons. Applying a drive signal has several advantages over other proposed means of accessing this desired regime of operation. The method of varying the magnetic field to tune from an initial regime of soft excitation to one of hard excitation has the disadvantage that the field cannot be changed rapidly. A drive signal, however, is well suited to starting a pulsed gyromonotron in the hard-excitation regime as described above. Another method involves controlling the voltage pulse to the electron gun to enable the gyromonotron to first start in the soft-excitation regime then end in a hard-excitation regime. This method does not have the flexibility of the one we propose, but it may be satisfactory.

4. *The ECRM oscillator plane*

The three regimes of qualitatively different behavior discussed above are shown on the ECRM oscillator plane of Fig. 14. This data is taken for a cavity no. 1 oscillation while directly injecting an rf signal. A premodulation experiment cannot be done (using our cavities) in this case because of the stability problems inherent in the prebunching cavities as the magnetic field and beam current are varied. Two current limits are identified in the experiment which delineate the different regions. The highest beam current possible while operating in the amplifier regime is termed $I_{\min}$. I_{start} is the measured start oscillation current of the ECRM oscillator in the absence of the external signal. The regimes shown are similar in location to that predicted.[45] With our short-cavity length (too short to produce beam-wave saturation), it is not possible to determine whether the high-efficiency region moves as predicted[45] to lower beam current in the presence of an external signal.

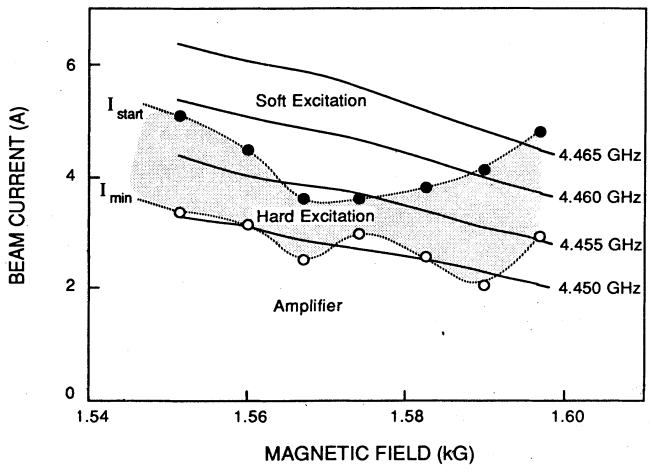

FIG. 14. ECRM oscillator plane showing contours of constant frequency when driven by external rf with drive frequency adjusted for maximum oscillator efficiency, $P_d = 12.5$ W, $V_{\text{cathode}} = 29.2$ kV, $V_{\text{mod-anode}} = 20.5$ kV.

Figure 14 also shows the operating frequency of the ECRM in both the oscillator and amplifier modes when driven at a constant power and at the frequency of maximum oscillator efficiency. It is found that the efficiency maximizes when the drive frequency equals the oscillation frequency (this will not necessarily be the case for larger drive power). An interesting feature of this figure is that the curves of constant frequency are continuous through the different regimes.

V. CONCLUSIONS

The general response of an electron cyclotron maser to the application of an external signal, applied both by direct injection of rf into the device and by premodulation of the electron beam, has been studied. It has been found that phase and frequency control can be achieved over the gyromonotron via phase locking. Phase locking the gyromonotron by premodulation of the electron beam produced results that far surpass those of any other locked oscillator system. This premodulation technique allowed phase locking at input power levels 15 dB below that predicted by Adler's theory for a single cavity. A perturbation theory has successfully predicted the phase-locking bandwidths for two- and three-cavity systems.

Three different regimes of ECRM behavior have been examined experimentally and located in the oscillator plane. It has been been shown that the regime of hard excitation can be accessed by application of a small external signal during the start up of the ECRM. Phase locking in the hard-excitation regime has also been demonstrated.

ACKNOWLEDGMENTS

The authors thank W. M. Bollen for construction of the gyroklystron and helpful discussions. We thank J. McAdoo for work on the phase diagnostics. H. P. Freund, R. K. Parker, and S. Y. Park are thanked for helpful discussions. The work of S. Swiadek and F. Wood on construction of the experiment is also gratefully acknowledged. This work was supported by the U.S. Office of Naval Research and the Office of Naval Technology.

APPENDIX: SMALL-SIGNAL GYROKLYSTRON THEORY WITH A TAPERED MAGNETIC FIELD

The objective here is to modify the linear multicavity theory presented in Ref. 13 to allow for small tapers of

the magnetic-field profile. The basic assumption is that the effect on the electrons of a change in magnetic field over any single cavity or drift section be small (comparable to the first-order electron interaction with the rf electric field). The change over the course of several sections, however, may be larger than first order. In each cavity the electron equation of motion is

$$\frac{d\mathbf{p}}{dt}+e\frac{\mathbf{p}\times(\mathbf{B}_{a_j}+\delta\mathbf{B})}{m_e\gamma}=-e\mathbf{E}\ , \tag{A1}$$

where the effects of the rf magnetic field are neglected. $\mathbf{E}$ is the rf electric field, and $\delta\mathbf{B}$ represents small variations of the static magnetic field about its average z component in the jth section $|\mathbf{B}_{a_j}|$. The complex notation

$$p_x+ip_y=ip_\perp\exp\{i[\Omega_{a_j}(t-t_0)+\phi]\}$$

is now used in Eq. (A1). Here the phase angles are shown in Fig. 2, $\Omega_{a_j}=e|\mathbf{B}_{a_j}|/(m\gamma_0)$ and $(\gamma_0-1)mc^2$ is the initial electron energy. The perpendicular components of (A1) yield Eqs. (10a) and (10b) for the evolution of magnitude $p_\perp$ and phase Λ of the slowly varying momentum. The magnetic-field variations are of the form given in Eq. (12). Expanding the electric field of Eq. (13) on the electron gyro-orbit (using Graf's addition theorem) Eqs. (10a) and (10b) can be written in terms of sums of cyclotron harmonics.[31] The relations between the cavity and gyro-orbit coordinates can be seen from Fig. 2,

$$\begin{aligned} y&=r\sin\theta=R_0\sin\theta_0+r_L\sin[\Omega(t-t_0)+\phi]\ ,\\ x&=r\cos\theta=R_0\cos\theta_0+r_L\cos[\Omega(t-t_0)+\phi]\ . \end{aligned} \tag{A2}$$

The modified versions of Eqs. (10a) and (10b) are now averaged over all time scales faster than $2\pi/(\omega-\Omega_{a_j})$, for interaction at the fundamental cyclotron harmonic, to yield equations for the slowly varying terms. An important point is the averaging of the magnetic variation parts of F_x and F_y [given in Eq. (11)]. Since the electron guiding center positions vary slowly (following a line of the slowly varying magnetic field) the variation parts of F_x and F_y vanish in the equation for $\dot{\Lambda}$ when averaged over the time scale $2\pi/\Omega_{a_j}$ [using Eqs. (A2)]. The slow-time-scale equations in a given cavity are now

$$\begin{aligned} \frac{dp_\perp}{dz}&=-\frac{e}{v_z}k_{ml}C_{ml}J_{m-1}(k_{ml}R_0)J_1'(k_{ml}r_L)F(z)\cos\Psi\\ &\quad+\frac{p_\perp}{2\gamma|\mathbf{B}_a+\delta B_z\hat{\mathbf{z}}|}\frac{d|\mathbf{B}|}{dz}\bigg|_{z=z_{\rm av}}\ , \end{aligned} \tag{A3}$$

$$\begin{aligned} \frac{d\Lambda}{dz}&=-\frac{e}{p_\perp v_z}k_{ml}C_{ml}J_{m-1}(k_{ml}R_0)\frac{J_1(k_{ml}r_L)}{k_{ml}r_L}F(z)\sin\Psi\\ &\quad+\frac{1}{v_z}\left[\omega-\frac{\Omega_a\gamma_0}{\gamma}\right]-\frac{e(z-z_{\rm av})}{\gamma m_e v_z}\frac{d|\mathbf{B}|}{dz}\bigg|_{z=z_{\rm av}}\ , \end{aligned}$$

where the prime indicates differentiation with respect to the argument and $\Psi=\Lambda-(m-1)\theta_0$. To progress further the equation of motion for the z component of the momentum Eq. (10c) must be solved. Applying Eqs. (A2) and again averaging over the time scale of the cyclotron motion Eq. (10c) becomes

$$\frac{dp_z}{dt}=-\frac{p_\perp^2}{2\gamma m_e|\mathbf{B}_a+\delta B_z\hat{\mathbf{z}}|}\frac{d|\mathbf{B}|}{dz}\bigg|_{z=z_{\rm av}}\ . \tag{A4}$$

Using energy conservation, the perpendicular momentum in (A4) may be written in terms of the axial momentum, the initial kinetic energy $\mathcal{E}_0$, and the energy exchanged with the rf field (assuming a weakly relativistic beam),

$$p_\perp^2=2m_e\mathcal{E}_0-p_z^2+2(m_ec)^2\delta\gamma\ ,$$

where $\delta\gamma=\gamma(z)-\gamma_0$. Here we linearize in the rf field interaction and will hence keep only first-order terms. Using the above in Eq. (A4) the axial velocity in the jth section of the device is

$$\begin{aligned} v_{z_j}(z)=v_{z_0}\Bigg[1-\frac{\alpha_0^2}{|\mathbf{B}_0|}\Bigg[\sum_{k=1}^{j-1}\frac{d|\mathbf{B}|}{dz}\bigg|_k L_k\\ +(z-z_{a_j})\frac{d|\mathbf{B}|}{dz}\bigg|_j\Bigg]\Bigg]^{1/2}\\ -\frac{v_{z_0}\delta\gamma}{\gamma_0}\ , \end{aligned} \tag{A5}$$

where L_k is the axial length of the kth section and $\mathbf{B}_0$ is the magnetic field at the entrance of the first cavity. The first part of v_z (under the radical) is merely due the conservation of electron magnetic moment. The second term comes from the change in electron energy due to interaction with the rf electric field. This will turn out to make a second-order (negligible) contribution to our results. Using Eq. (A5) in Eqs. (A3) and neglecting terms involving multiplication of $\delta\gamma$ with the small magnetic-field change over a given section:

$$\delta\gamma\left[\frac{d|\mathbf{B}|}{dz}\bigg|_j\Big/|\mathbf{B}_0|\right]L_j\ll 1\ ,$$

a single equation for the complex momentum $p=p_\perp e^{-i\Lambda}$ in the jth section can be written,

$$\begin{aligned} \left[\frac{d}{dz}+i\Delta_j(z)\right]p&=-\frac{ek_{ml}C_{ml}}{2v_{z_j}}J_{m-1}(k_{ml}R_0)F(z)\\ &\quad\times e^{-i(m-1)\theta_0}\ , \end{aligned} \tag{A6}$$

where m and l are the mode indices in the jth section and the detuning factor has been defined

$$\begin{aligned} \Delta_j(z)&=\frac{\left[\omega-\dfrac{\Omega_{a_j}\gamma_0}{\gamma}-\dfrac{\Omega_{a_j}(z-z_{a_j})}{|\mathbf{B}_{a_j}|}\dfrac{d|\mathbf{B}|}{dz}\bigg|_j\right]}{v_{z_j}\left[1-\left[\dfrac{\Delta v_{z_j}}{v_{z_j}}\right]^2\right]^{1/2}}\\ &\quad+\frac{i\dfrac{d|\mathbf{B}|}{dz}\bigg|_j}{2|\mathbf{B}_j(z)|}\ . \end{aligned}$$

The definition for the velocity at the start of the jth section is

$$v_{z_j}(z)=v_{z_0}\left[1-\frac{\alpha_0^2}{|\mathbf{B}_0|}\sum_{k=1}^{j-1}L_k\left.\frac{d|\mathbf{B}|}{dz}\right|_k\right]^{1/2}$$

and the following abbreviations have been used in both the above equations:

$$\mathbf{B}_j(z)=\mathbf{B}_{a_j}+(z-z_{a_j})\left.\frac{d\mathbf{B}}{dz}\right|_j$$

and

$$\Delta v_{z_j}=v_{z_0}\alpha_0\left[\frac{(z-z_{a_j})}{|\mathbf{B}_0|}\left.\frac{d|\mathbf{B}|}{dz}\right|_j\right]^{1/2}.$$

Here α is the ratio of the perpendicular-to-parallel electron velocity, and two of the Bessel functions have been replaced by their small argument expansions ($k_{mn}r_L \ll 1$) in order to arrive at Eq. (A6). The solution to the ordinary differential equation of Eq. (A6) can be easily found and is given in Ref. 13.

The rf fields are assumed to be generated by the external signal in the first cavity but are solved using self-consistent iterations in the following cavities. Using the same normalization scheme as in the text,

$$\bar{p}=\frac{p}{m_e c},\quad \bar{F}=\frac{eF}{m_e c^2},\quad \beta=\frac{v_z}{c},\quad \bar{z}=\frac{z}{\lambda_0},$$

$$\bar{\Omega}=\frac{\Omega\lambda_0}{c},\quad \bar{B}=\frac{B\lambda_0 e}{m_e c},$$

etc. an initial condition of $\bar{p}=\bar{p}_{\perp_0}e^{-i\phi_0}$ and an electric-field profile in the first cavity of $\bar{F}=\bar{F}_1\sin\bar{k}_{z_1}(\bar{L}_1-\bar{z})$ (where $\bar{L}_1$ and $\bar{k}_{z_1}$ are the normalized length and axial wave number) the momentum at the end of the first cavity is

$$\bar{p}(\bar{z}=\bar{L}_1,\phi_0)=\bar{p}_{\perp_0}\left[1+\left.\frac{d|\bar{\mathbf{B}}|}{d\bar{z}}\right|_1\frac{\bar{L}_1}{|\bar{\mathbf{B}}_0|}\right]^{1/2}\left[1-\frac{\langle\beta_1\rangle_{v_{z_0}}}{\beta_1}\frac{\bar{E}_1}{\bar{p}_{\perp_0}}e^{-i(m_1-1)\theta_0}e^{i\phi_0}R_1\right]$$
$$\times e^{-i(\phi_0+M_1)}\exp\left[i\frac{\bar{p}_{\perp_0}\bar{\omega}}{\gamma_0^2\beta_1}\mathrm{Re}\left[\frac{\langle\beta_1\rangle_{v_{z_0}}}{\beta_1}e^{i\phi_0}T_1\bar{E}_1e^{-i(m_1-1)\theta_0}\right]\right],\tag{A7}$$

where $\bar{E}_1$ is related to F_1 by the proportionality constant given in Eq. (24). R_1 and T_1 are defined

$$R_1=\frac{1}{D_1}\{\bar{k}_{z_1}[\cos(\bar{k}_{z_1}\bar{L}_1)-\cos(\Delta_1^0\bar{L}_1)]+i[\Delta_1^0\sin(\bar{k}_{z_1}\bar{L}_1)-\bar{k}_{z_1}\sin(\Delta_1^0\bar{L}_1)]\},\tag{A8}$$

$$T_1=\frac{1}{D_1^2}[(\Delta_1^{0^2}-\bar{k}_{z_1}^2)\bar{k}_{z_1}\bar{L}_1\cos(\bar{k}_{z_1}\bar{L}_1)+(\Delta_1^{0^2}+\bar{k}_{z_1}^2)\sin(\bar{k}_{z_1}\bar{L}_1)-2\Delta_1^0\bar{k}_{z_1}\sin(\Delta_1^0\bar{L}_1)]$$
$$+\frac{i}{D_1^2}\{(\Delta_1^{0^2}-\bar{k}_{z_1}^2)\Delta_1^0\bar{L}_1\sin(\bar{k}_{z_1}\bar{L}_1)+2\Delta_1^0\bar{k}_{z_1}[\cos(\Delta_1^0\bar{L}_1)-\cos(\bar{k}_{z_1}\bar{L}_1)]\},\tag{A9}$$

where $D_1=(\Delta_1^{0^2}-\bar{k}_{z_1}^2)$. M_1 is given by

$$M_1=\frac{\bar{\Omega}_1\beta_1\bar{L}_1\gamma_0^2}{3\bar{p}_{\perp_0}^2 f_1}[(2+f_1)\sqrt{1-f_1}-(2-f_1)\sqrt{1+f_1}]+\frac{(\bar{\omega}-\bar{\Omega}_1)\bar{L}_1}{\beta_1 f_1}(\sqrt{1+f_1}-\sqrt{1-f_1})$$

where f_1 is defined

$$f_1=\frac{\bar{p}_{\perp_0}^2}{2|\bar{\mathbf{B}}_0|\gamma_0^2\beta_1^2}\left.\frac{d|\bar{\mathbf{B}}|}{d\bar{z}}\right|_1\bar{L}_1.$$

The effect of the tapered magnetic field can be seen from Eq. (A7) to merely vary the magnitude of the perpendicular momentum by conservation of the electron magnetic moment and to advance or retard the gyrophase due to the change in cyclotron frequency. In the first drift section (of length $\bar{L}_2$) there is no rf electric field and the electrons ballistically bunch and conserve magnetic moment in the tapered magnetic field. The solution for momentum at the end of the first cavity can be propagated forward to the end of the drift section by the relation:

$$\bar{p}(\bar{z}=\bar{L}_1+\bar{L}_2,\phi_0)=\bar{p}(\bar{z}=\bar{L}_1,\phi_0)\left[1+\left.\frac{d|\bar{\mathbf{B}}|}{d\bar{z}}\right|_2\frac{\bar{L}_2}{|\bar{\mathbf{B}}_2|}\right]^{1/2}e^{-iM_2}\exp\left[i\frac{\bar{p}_{\perp_0}\bar{\omega}\bar{L}_2}{\gamma_0^2\beta_2}\mathrm{Re}\left[\frac{\langle\beta_1\rangle_{v_{z_0}}}{\beta_1}e^{i\phi_0}R_1\bar{E}_1e^{-i(m_1-1)\theta_0}\right]\right],$$

where the equation of motion Eq. (A6) is again solved, this time with $F(z)=0$. $\mathbf{B}_2$ is the magnetic field at the entrance to section two. To determine the current density of Eq. (15), the momentum must be averaged over initial conditions. The average over initial gyrophase ϕ_0 yields

$$\langle \bar{p}(\bar{z}=\bar{L}_1+\bar{L}_2)\rangle_{\phi_0}=i\bar{p}_{\perp_0}e^{-i(M_1+M_2-\hat{\delta}_1)}\prod_{j=1}^{2}\left[1+\frac{d|\bar{\mathbf{B}}|}{d\bar{z}}\bigg|_j\frac{\bar{L}_j}{|\bar{\mathbf{B}}_j|}\right]^{1/2}\left[J_1(X_{11})+i\frac{\bar{E}_1R_1}{\bar{p}_{\perp_0}}\frac{\langle\beta_1\rangle_{v_{z_0}}}{\beta_1}J_0(X_{11})e^{-i\hat{\delta}_1}\right]$$

at the end of the first drift section where the bunching parameter is defined,

$$X_{11}=\frac{\bar{\omega}\bar{p}_{\perp_0}}{\gamma_0^2}\frac{\langle\beta_1\rangle_{v_{z_0}}}{\beta_1}\left|\bar{E}_1\left[\frac{T_1}{\beta_1}+\frac{\bar{L}_2R_1}{\beta_2}\right]\right|,$$

and where

$$\hat{\delta}_1=\sigma_{11}=\arg(\bar{E}_1)+\arg\left[\frac{T_1}{\beta_1}+\frac{\bar{L}_2R_1}{\beta_2}\right].$$

In all subsequent cavities the electric field is calculated from the ac beam current density. The electrons are assumed to perturb only the longitudinal structure of the electric field. The wave equation, for a single electromagnetic mode, is

$$\left[\frac{d^2}{d\bar{z}^2}-\bar{k}_{ml}^2+\bar{\omega}^2\left[1+\frac{1}{Q_0}-\frac{i}{Q_L}\right]\right]\bar{E}=-i\bar{I}\left\langle\frac{\bar{p}}{\gamma}e^{i(m-1)\theta_0}\right\rangle_{\phi_0,\theta_0,t_0,v_{z_0}},$$

with solution in the jth section[13]

$$\bar{E}_j(\bar{z}+\bar{z}_j)=-i\frac{\bar{I}_j\left\langle\frac{\bar{p}(\bar{z}_j)}{\gamma}e^{j(m_j-1)\theta_0}\right\rangle_{\phi_0,\theta_0,t_0,v_{z_0}}}{\bar{k}_{z_j}^2\sin[\bar{k}_{z_j}(\bar{z}-\bar{L}_j)]}\{\sin[\bar{k}_{z_j}(\bar{z}-\bar{L}_j)]+\sin(\bar{k}_{z_j}\bar{L}_j)-\sin(\bar{k}_{z_j}\bar{z})\},\tag{A10}$$

where $\bar{I}_j$ is defined in Eq. (26) and $\bar{k}_{z_j}$ is

$$\bar{k}_{z_j}^2=\bar{\omega}^2\left[1+\frac{1}{Q_{0_j}}-\frac{i}{Q_{L_j}}\right]-\bar{k}_{m_jl_j}^2.$$

The momentum used in evaluating Eq. (A10) is that at the start of the jth section. The electric field of Eq. (A10) is now used in the momentum equation (A6). These new momenta could be used to generate a new electric field, etc., but the iteration is stopped at this point. From this point onwards the calculation proceeds as through the first two sections. In this way the generalized formulas for electron momenta through the prebuncing sections are calculated. The linearized transverse electron momenta at the entrance to the $(k+1)$st cavity (after k prebunching stages) is

$$\bar{p}(\bar{z}_{K+1},\phi_0,\theta_0,t_0,v_{z_0})=\bar{p}_{\perp_0}\exp\left[-i\sum_{j=1}^{2K}M_j\right]\prod_{j=1}^{2K}h_je^{-i[\psi_{K+1}+(m_{K+1}-1)\theta_0]}\left[1-\sum_{j=1}^{K}\frac{\langle\beta_{2j-1}\rangle_{v_{z_0}}}{\beta_{2j-1}}\frac{\bar{E}_jR_j}{\bar{p}_{\perp_0}}\frac{\prod_{n=2j-1}^{2K}h_n}{\prod_{n=1}^{2K}h_n}\right],$$

where h_j, $\bar{E}_j$, and M_j are given in the text in Eqs. (21), (25), and (20), respectively, and

$$R_j=\frac{1}{\Delta_k^{0^2}-\bar{k}_{z_j}^2}\left[\frac{1}{\bar{k}_{z_j}}\tan\left[\frac{\bar{k}_{z_j}\bar{L}_k}{2}\right](e^{i\Delta_k^0\bar{L}_k}+1)-\frac{i}{\Delta_k^0}(e^{i\Delta_k^0\bar{L}_k}-1)\right],\tag{A11}$$

$$T_j=\frac{1}{\bar{k}_{z_j}^2}\left[\frac{\bar{k}_{z_j}}{\Delta_k^0}\frac{\Delta_k^0\bar{L}_k\tan(\bar{k}_{z_j}\bar{L}_k/2)-i\bar{k}_{z_j}\bar{L}_k}{\Delta_k^{0^2}-\bar{k}_{z_j}^2}-\frac{e^{i\Delta_k^0\bar{L}_k}-1}{\Delta_k^{0^2}}\right]$$
$$+\frac{2ie^{i/2\Delta_k^0\bar{L}_k}}{\bar{k}_{z_j}^2(\Delta_k^{0^2}-\bar{k}_{z_j}^2)^2}[(\Delta_k^{0^2}+\bar{k}_{z_j}^2)\sin(\Delta_k^0\bar{L}_k/2)-2\Delta_k^0\bar{k}_{z_j}\cos(\Delta_k^0\bar{L}_k/2)\tan(\bar{k}_{z_j}\bar{L}_k/2)],\tag{A12}$$

where the subscript $k=2j-1$ and $\bar{k}_{z_j}$ is the axial wave number in the jth stage.

The bunching phase is given by

$$\psi_1=\phi_0-\omega t_0-(m_1-1)\theta_0,$$

$$\psi_j=\phi_0-\omega t_0-\hat{x}_{j-1}\cos(\psi_1+\hat{\delta}_{j-1})-(m_j-1)\theta_0,$$

where $\hat{\delta}_j$ is

$$\hat{\delta}_j = \arctan\left[\sum_{k=1}^{j}\sum_{s=k}^{j} X_{ks}\sin\xi_{ks} \Big/ \sum_{k=1}^{j}\sum_{s=k}^{j} X_{ks}\cos\xi_{ks}\right] \quad \text{for } j>1$$

and

$$\hat{x}_j = e^{-i\hat{\delta}_j}\sum_{k=1}^{j}\sum_{s=k}^{j} x_{ks}e^{i\xi_{ks}} \quad \text{where } \xi_{ks}=\sigma_{ks}+(m_1-m_k)\theta_0$$

and x_{ks} and σ_{ks} are given by Eqs. (22) and (23), respectively. A final relationship, necessary in finding the beam-generated electric field, is the electron energy change through N prebunching cavities:

$$\delta\gamma_N = -\frac{\bar{p}_{\perp_0}}{\gamma_0}\mathrm{Re}\left[\sum_{j=1}^{N}\frac{\langle\beta_{2j-1}\rangle_{v_{z_0}}}{\beta_{2j-1}}\bar{E}_j R_j e^{i\psi_j}\prod_{n=1}^{2j-2} h_n\right]. \tag{A13}$$

---

*Present address: Department of Electrical Engineering/Electrophysics, University of Southern California, Los Angeles, CA 90089-0271.

[1]A. V. Gaponov, M. I. Petelin, and V. K. Yulpatov, Radiophys. Quantum Electron. **10**, 794 (1967).
[2]K. E. Kreischer and R. J. Temkin, Phys. Rev. Lett. **59**, 547 (1987).
[3]A. Gol'denberg, A. Pavel'yev, and V. Khizhnyak, in Proceedings of the Twelfth International Conference on Infrared and Millimeter Waves, Lake Buena Vista, Florida, 1987 (unpublished).
[4]K. Felch *et al.*, in *Conference Digest of the Eleventh International Conference on Infrared and Millimeter Waves, Pisa, Italy, 1986,* edited by G. Moruzzi (ETS Editrice, Pisa, Italy, 1986), p. 229.
[5]E. M. Demidovich, C. S. Kovalev, A. A. Kuryev, and F. G. Shevchenko, Radio Eng. Electron. Phys. **18**, 1542 (1973).
[6]See, for example, R. S. Symons and H. R. Jory, in *Advances in Electronic and Electron Physics,* edited by L. Marton and C. Marton (Academic, New York, 1981), Vol. 55, p. 1.
[7]A. H. McCurdy *et al.*, Phys. Rev. Lett. **57**, 2379 (1986).
[8]A. K. Ganguly and K. R. Chu, Int. J. Electron. **51**, 503 (1981).
[9]V. S. Ergakov and M. A. Moiseev, Izv. Vyssh. Uchebn. Zaved. Radiofiz. **18**, 120 (1975).
[10]A. V. Gaponov *et al.*, Int. J. Electron. **51**, 277 (1981).
[11]Y. Carmel *et al.*, Phys. Rev. Lett. **50**, 112 (1983).
[12]W. M. Manheimer, Int. J. Electron. **63**, 29 (1987).
[13]A. K. Ganguly, A. W. Fliflet, and A. H. McCurdy, IEEE Trans. Plasma Sci. **PS-13**, 409 (1985).
[14]A. H. McCurdy and C. M. Armstrong, IEEE Trans. Microwave Theory Tech. **36**, 891 (1988).
[15]V. S. Bazhanov, V. S. Ergakov, and M. A. Moiseev, Radiophys. Quantum Electron. **20**, 90 (1977).
[16]W. M. Bollen *et al.*, IEEE Trans. Plasma Sci. **PS-13**, 417 (1985).
[17]Anaren Microwave Components, Cat. No. 17, 197 (1984).
[18]B. van der Pol, Philos. Mag. **III**, 65 (1927).
[19]E. V. Appleton, Proc. Camb. Philos. Soc. **21**, 231 (1923).
[20]R. Adler, Proc. IRE **34**, 351 (1946).
[21]J. C. Slater, Mass. Inst. Technol. Res. Lab. Electron. Tech. Rep. **35** (1947).
[22]K. Kurokawa, Proc. IEEE **61**, 1386 (1973).
[23]H. L. Stover and W. H. Steier, Appl. Phys. Lett. **8**, 91 (1966).
[24]M. Sargent III, M. O. Scully, and W. E. Lamb, Jr., *Laser Physics* (Addison-Wesley, Reading, MA, 1974), pp. 120–141.
[25]J. C. Slater, *Microwave Electronics* (Van Nostrand, New York, 1950), p. 205.
[26]W. E. Lamb, Jr., Phys. Rev. A **134**, 1429 (1964).
[27]G. S. Nusinovich, Int. J. Electron. **51**, 457 (1981).
[28]A. W. Fliflet, M. E. Read, K. R. Chu, and R. Seeley, Int. J. Electron. **53**, 505 (1982).
[29]P. Sprangle, C. M. Tang, and W. M. Manheimer, Phys. Rev. A **21**, 302 (1980).
[30]E. E. David, Jr., Proc. IRE **40**, 669 (1952).
[31]J. E. Evans, R. C. Fletcher, F. F. Rieke, Mass. Inst. Technol. Rad. Lab. Rep. **1051** (1946).
[32]H. Pollmann and B. G. Bosch, IEEE Trans. Electron Dev. **ED-14**, 609 (1967).
[33]D. M. Brookbanks, in Proceedings of the Conference on Military Microwaves, London, England, 1982 (unpublished).
[34]D. Anderson, M. Lisak, and T. Lewin, IEEE Trans. Microwave Theory Tech. **MTT-31**, 963 (1983).
[35]J. C. Slater, *Micronotes 4* (Microwave Associates, Burlington, MA, 1966), p. 1.
[36]B. Vyse, V. H. Smith, and M. O. White, in Ref. 33.
[37]B. Vyse and H. Levinson, IEEE Trans. Microwave Theory Tech. **MTT-29**, 739 (1981).
[38]D. M. Guillory and R. W. McMillan, in *Conference Digest of the Tenth International Conference on Infrared and Millimeter Waves, Lake Buena Vista, Florida, 1985,* edited by R. J. Temkin (IEEE, New York, 1985), p. 48.
[39]M. E. Read, R. Seeley, and W. M. Manheimer, IEEE Trans. Plasma Sci. **PS-13**, 398 (1985).
[40]E. M. Dewan, IEEE Trans. Autom. Control **AC-17**, 655 (1972).
[41]N. Minorsky, *Nonlinear Oscillations* (Van Nostrand, Princeton, NJ, 1962), p. 71.
[42]D. S. Furuno, D. B. McDermott, N. C. Luhmann, Jr., and P. Vitello, Int. J. Electron. **57**, 1151 (1984).
[43]P. Sprangle and A. T. Drobot, IEEE Trans. Microwave Theory Tech. **MTT-25**, 528 (1977).
[44]N. N. Bogoliubov and Y. A. Mitropolsky, *Asymptotic Methods in the Theory of Nonlinear Osillations* (Hindustan, Delhi, 1961), pp. 91–102.
[45]V. S. Yergakov, M. A. Moiseyev, and V. I. Khizhnyak, Radio Eng. Electron. Phys. **23**, 9 (1978).

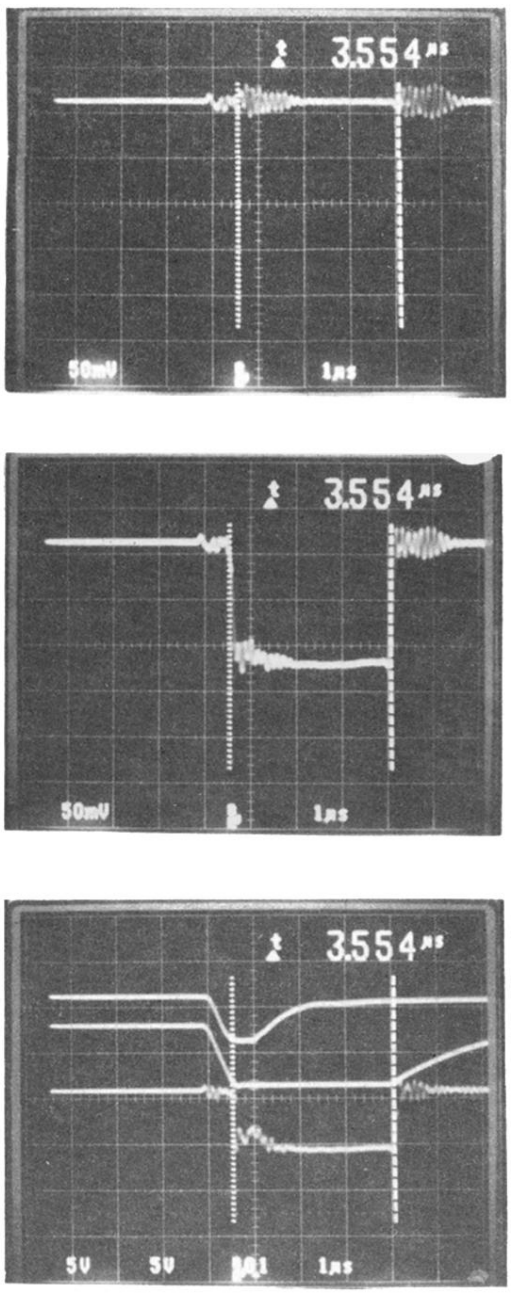

FIG. 11. Oscillographs of crystal diode traces monitoring ECRM oscillator output rf power in hard-excitation regime. (a) $P_d = 0$, no external signal applied; (b) $P_d = 286$ mW, excitation of 12.1 kW oscillation with drive frequency equal to oscillation frequency; (c) synchronization of (from top) drive rf pulse, electron-gun high-voltage pulse, and output rf oscillation.